ENGINEERING

Organoid microphysiological system preserves pancreatic islet function within 3D matrix

S. N. Patel[1]*, M. Ishahak[2]*, D. Chaimov[1], A. Velraj[1], D. LaShoto[1], D. W. Hagan[1], P. Buchwald[3,4], E. A. Phelps[1], A. Agarwal[2,3†], C. L. Stabler[1,5†]

Three-dimensional (3D) multicellular organoids recapitulate the native complexities of human tissue better than traditional cellular monolayers. As organoids are insufficiently supported using standard static culture, microphysiological systems (MPSs) provide a key enabling technology to maintain organoid physiology in vitro. Here, a polydimethylsiloxane-free MPS that enables continuous dynamic culture and serial in situ multiparametric assessments was leveraged to culture organoids, specifically human and rodent pancreatic islets, within a 3D alginate hydrogel. Computational modeling predicted reduced hypoxic stress and improved insulin secretion compared to static culture. Experimental validation via serial, high-content, and noninvasive assessments quantitatively confirmed that the MPS platform retained organoid viability and functionality for at least 10 days, in stark contrast to the acute decline observed overnight under static conditions. Our findings demonstrate the importance of a dynamic in vitro microenvironment for the preservation of primary organoid function and the utility of this MPS for in situ multiparametric assessment.

INTRODUCTION

The practice of in vitro cell culture on static, two-dimensional (2D) glass or polystyrene surfaces has provided the foundation for numerous biomedical discoveries over the past century. The inability of these culture systems to recapitulate critical human in vivo physiological responses, however, has been well documented (*1*, *2*). Replacement of human cell monolayers with 3D organoids, procured from biopsies, cadaveric organ donations, or the self-organization of cultured pluripotent stem cells, provides superior in vitro models for the investigation of complex biological phenomenon and the effective screening of emerging pharmaceuticals (*3*). For example, 3D multicellular pancreatic islets of Langerhans are considered widely superior to β cell monolayers for studying pancreatic physiology and diabetes, as well as for drug screening and cellular transplantation (*4*, *5*).

Maintaining and interrogating organoids such as pancreatic islets in vitro, however, are exceptionally challenging. The current standard protocol for culturing primary islets (i.e., static culture in a flask or petri dish under low seeding densities) is suboptimal, resulting in substantial temporal declines in cell mass and function (*6*). This can be partly attributed to both the loss of native 3D microarchitecture and deficient nutritional delivery in vitro (*7*). As a result, the utility of islet organoids for pharmaceutical screenings, biological studies, and transplantation therapies is extremely limited. Overcoming these challenges has proven difficult because of the complexity of developing in vitro culture systems that provide key features of the in vivo environment, such as a 3D support matrix and a sufficient supply of nutrients, while retaining ease of use in a general laboratory setting.

Hydrogels made from synthetic or natural-based materials have been used to provide 3D support of organoids (*8*). Alginate, a seaweed-derived polysaccharide, has been extensively studied for 3D encapsulation of cells due to its low toxicity, ease of gelation, and tunable properties (*9*). Because of its inert nature and biostability, the in vitro immobilization of cells within an alginate hydrogel also facilitates cell-specific spatiotemporal imaging and tracking during extended culture periods. However, embedding organoids within 3D hydrogels creates an additional barrier to the diffusion of solutes, resulting in decreased nutrient delivery during conventional static culture. For organoids with high metabolic activity, such as islets, static culture in a bulk 3D matrix is highly unsuitable for maintaining long-term cell viability and function (*6*).

Dynamic culture systems, such as stirred flasks, rotating wall vessels, hollow fibers, and direct perifusion chambers, can improve mass transport for effective nutrient delivery and waste removal (*10*). The widespread implementation of these approaches for organoid culture is hindered by their large culture media volumes and limited compatibility with existing assays. Microphysiological systems (MPSs), such as organs-on-chips, have the potential to address these challenges by decreasing the culture scale and facilitating the integration of sensors, functional readouts, and optical monitoring (*11*). These microfluidic devices are commonly fabricated from polydimethylsiloxane (PDMS), a noncytotoxic silicone polymer (*12*). However, the fabrication of PDMS-based MPS requires highly specialized photolithography facilities, and the inherent size restrictions of this method create challenges in developing MPS for organoid culture (*13*).

Substituting PDMS for poly(methyl methacrylate) (PMMA) as the manufacturing material, we engineered an MPS platform for the long-term continuous dynamic culture of organoids within a 3D hydrogel. Rodent- and human-derived islets were embedded in alginate and integrated into our MPS or cultured using traditional methods. The impact of the culture systems on islet health was temporally assessed and compared, both in silico and in vitro. We further demonstrated the ability to perform temporal noninvasive tracking of specific islets in response to standard or stimulated culture

[1]J. Crayton Pruitt Family Department of Biomedical Engineering, University of Florida, Gainesville, FL 32611, USA. [2]Department of Biomedical Engineering, University of Miami, Coral Gables, FL 33146, USA. [3]Diabetes Research Institute, University of Miami Miller School of Medicine, Miami, FL 33136, USA. [4]Department of Molecular and Cellular Pharmacology, University of Miami Miller School of Medicine, Miami, FL 33136, USA. [5]University of Florida Diabetes Institute, Gainesville, FL 32610, USA.
*These authors contributed equally to this work.
†Corresponding author. Email: a.agarwal2@miami.edu (A.A.); cstabler@bme.ufl.edu (C.L.S.)

conditions, with additional dynamic characterization of islet function within our MPS platforms. To our knowledge, our study is the first to demonstrate serial, dynamic assessment of the same set of islets over extended culture periods, with both off-line functional assessment of dynamic glucose-stimulated insulin secretion (dGSIS) and simultaneous in situ tracking of viability and calcium signaling. With the establishment of a successful 3D islet organoid culture system using our MPS, leveraging this platform for the study of diabetes pathogenesis and the screening of diabetic pharmaceutical agents is discussed.

RESULTS

Organoid MPS development and implementation

The organoid MPS used in this study was optimized from our previously described fluidic chip (*14*). The original fluidic chip, referred to as the Acry-Chip, was fabricated entirely from PMMA and contained geometric features (i.e., an inlet chamfer and an obstacle) in the flow path designed to deliver predictable and optimized convective transport into the culture well (Fig. 1A). To explore the benefits of enhanced oxygenation in the culture niche, we developed an alternative chip design that replaced the PMMA base of the culture well with an oxygen-permeable perfluoroalkoxy (PFA) membrane, referred herein as the Oxy-Chip (Fig. 1B). Chips were fabricated to the specifications of 3D computer-aided design (CAD) models using a subtractive rapid prototyping approach, which used a combination of computer numerical control (CNC) micromilling and CO_2 laser cutting. A thru-hole was milled into the culture wells, and the PFA membrane was adhered to the bottom piece (Fig. 1C). The top piece contained embedded gaskets for reproducible sealing of the culture wells. The final assembled Oxy-Chip consisted of three independent, fluidically sealed, and optically clear culture niches (Fig. 1D). The Oxy-Chip was further modified to incorporate fiber-optic oxygen sensors to characterize the oxygen permeability of the PFA membrane (fig. S1, A and B). On the basis of oxygen measurements (Fig. 1E), the oxygen diffusion coefficient through the 25-μm-thick PFA membrane was calculated as 56 ± 5 $\mu m^2/s$ (n = 5; fig. S1C), a 1.2% difference from the theoretical predictions.

A streamlined workflow was developed to facilitate the implementation of the organoid MPS (Fig. 1F). First, primary islets within a hydrogel matrix were manually loaded into the open culture wells of the bottom chip piece. After placement of the top piece, a commercially available chip holder was used to seal the two pieces and integrate fluidic connections. Each well was then independently perifused with recirculating media using a peristaltic pump in a standard cell culture incubator (37°C, 5% CO_2). For in situ functional (i.e., cellular secretion) or optical (i.e., bright field and/or fluorescent) assessment, the fluidic connections and form factor of the organoid MPS were designed to be compatible with existing laboratory equipment, such as a dynamic perifusion system or a confocal fluorescent microscope.

In silico modeling of islet physiology within the organoid MPS

The impact of the organoid MPS on cultured hydrogel-embedded islets was first investigated in silico using a 2D finite element method (FEM) model of islet physiology (*15*). We hypothesized that continuous perifusion of oxygenated media and the integration of the

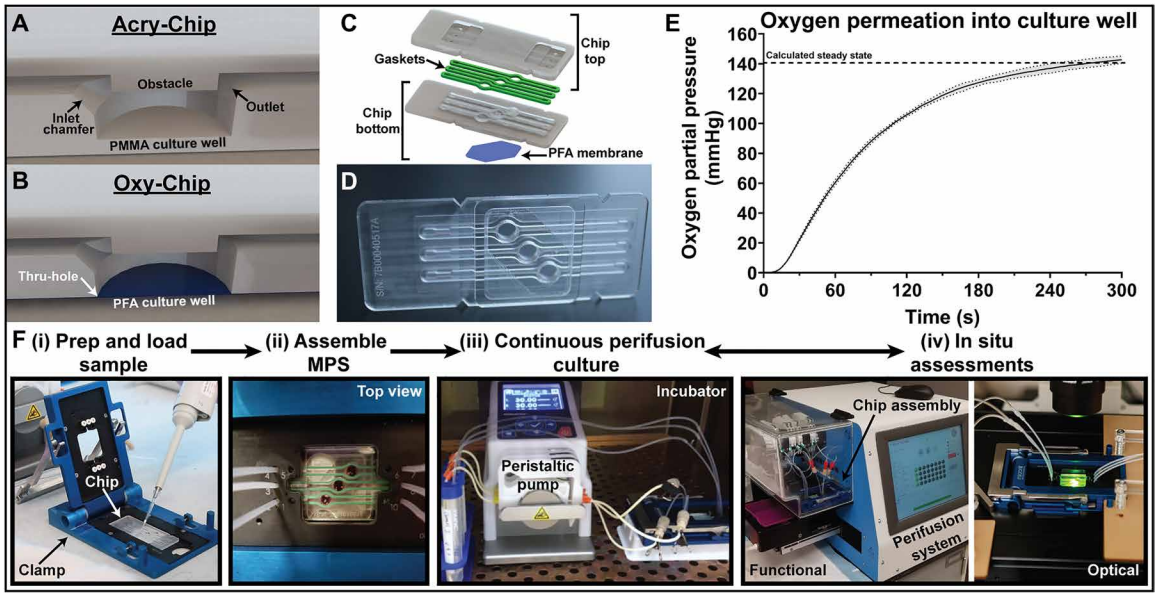

Fig. 1. Design validation of islet MPS. (**A**) 3D CAD render of organoid MPS with PMMA bottom (Acry-Chip) and features for optimized fluid transport. (**B**) 3D CAD render of modified organoid MPS chip with a thru-hole and PFA membrane (Oxy-Chip) to enable oxygen permeability in the culture well. (**C**) Exploded view of 3D CAD render of Oxy-Chip, composed of a chip top with embedded gaskets to create a fluidic seal and a chip bottom with a PFA membrane for oxygen permeability. (**D**) Fully fabricated Oxy-Chip bottom with thru-holes sealed by optically clear PFA membrane. (**E**) Oxygen partial pressure in the culture well of Oxy-Chip reaches calculated steady-state value, determined using the estimated diffusion coefficient of oxygen in PFA. The shaded area indicates SD values corresponding to its means (n = 5). (**F**) Schematic representation of experimental workflow, where (i) organoids and hydrogel were prepared and manually loaded into the wells of the chip, (ii) the chip was sealed and fluidic connections were introduced when the MPS was assembled in the chip holder, (iii) the organoid MPS was placed in an incubator with a pump for continuous perifusion culture, and (iv) the MPS can be temporarily removed from culture to perform a dynamic functional assay or for optical assessment(s). Photo credit: Smit N Patel, University of Florida; Matthew Ishahak, University of Miami.

oxygen-permeable membrane would increase local oxygen supply to the islets, resulting in decreased cellular hypoxia and downstream impacts on insulin secretion. The model consisted of 10 rodent islet equivalents (IEQs) discreetly distributed throughout the hydrogel. IEQ provides a standardized estimate of islet volume, with one IEQ corresponding to the volume of a perfectly spherical islet with a diameter of 150 μm (*16*). Size characterization of the handpicked islets used in our subsequent studies validated this assumption, with an average diameter of 173 ± 87 μm (n = 629; fig. S2A). Despite the simplification of biologic variability, the computational model provides a reasonable approximation of expected phenomenon.

To interrogate the impact of flow and flow rate on islet function, we developed computational models of the three culture platforms: (i) 48-well plate (standard control), (ii) Acry-Chip MPS, and (iii) Oxy-Chip MPS (fig. S1, D to H). Because of the small volume of culture media, MPS platforms exhibited decreased oxygen availability under static culture conditions (fig. S1D). Adding perifusion to the MPS platforms (at rates from 10 to 100 μl/min) substantially increased oxygen delivery to the islets (fig. S1E). To globally capture potential oxygen impacts on islet function, the functional islet area (i.e., the percentage of islet area above the hypoxia-induced dysfunction threshold of 5.1×10^{-4} mol/m^3) was calculated (*17*). While static MPS culture resulted in a function islet area statistically equivalent to standard 48-well culture (fig. S1F), the dynamic flow within Acry-Chip and Oxy-Chip caused significantly elevated functional islet area (fig. S1G). Flow models identified 30 μl/min as the optimal flow rate, as this rate delivered a functional islet area statistically equivalent to the higher flow rates (fig. S1G) with a minimal shear stress at the islet boundaries (fig. S1H).

Comparing standard static culture to MPS platforms (30 μl/min of flow rate) revealed spatially distinct oxygen concentration gradients (Fig. 2A). For the static model, classic oxygen gradients were observed, with a negative correlation between oxygen concentration and the islet's distance from the surface of the bathing media. In the perifusion culture models, the concentration gradient followed the fluid flow path, where oxygen levels were reduced in the region furthest away from the fluidic inlet. The average intra-islet oxygen concentration after 24 hours of simulated culture was an order of magnitude higher in the Acry-Chip continuous perifusion model (0.02 mol/m^3) when compared to the static model (0.002 mol/m^3). The addition of the oxygen-permeable membrane within the MPS (Oxy-Chip) further elevated oxygen delivery, resulting in an additional twofold increase in average oxygen levels (0.04 mol/m^3). In rodent islets, the in vivo oxygen tension has been reported to be approximately 0.07 mol/m^3, but up to 25% of normal rodent islets may experience oxygen tension below 0.02 mol/m^3 (*18*, *19*). As a result, the in silico models suggest that continuous perifusion culture within the MPS provides a more physiologically relevant microenvironment than static culture.

While acute exposure to hypoxia has been shown to impair glucose-stimulated insulin secretion, substantial cell death may not occur (*20*, *21*). This was accounted for in the model by deactivating the insulin production and secretion functions in islet regions where oxygen was below the hypoxia-induced dysfunction threshold. As shown (Fig. 2B), the simulated functional islet area at 24 hours was significantly higher in the Oxy-Chip (98.6 ± 4.1%) than in the static culture model (53.9 ± 27.4%; P = 0.001), while the Acry-Chip was predicted to functionally support an intermediate percentage of islets (78.3 ± 22.7%). Models also predicted a more homogenous distribution of oxygen in the Oxy-Chip, with reduced variability in functional islet area (F test between the three conditions of P = 0.0002). Simulations of insulin release in response to a high glucose challenge

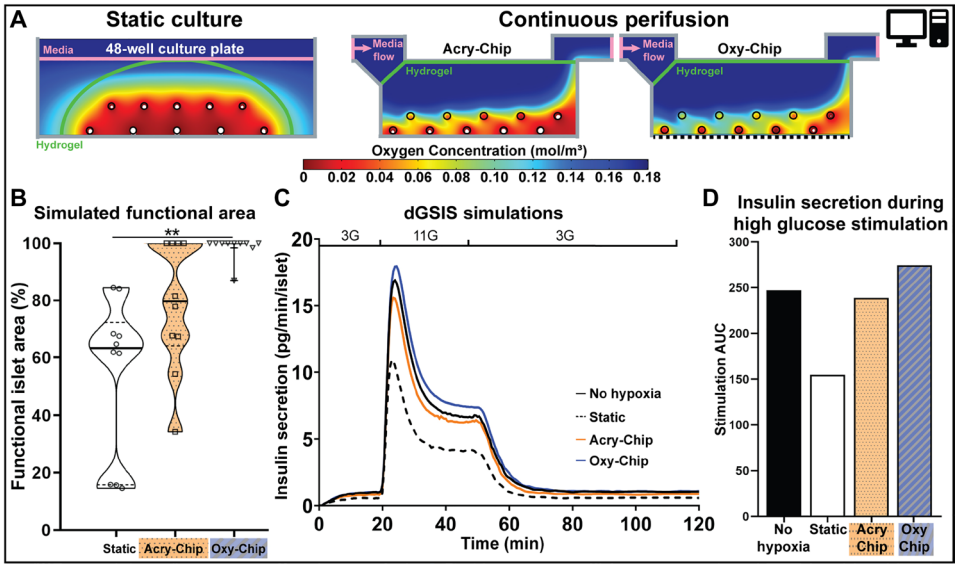

Fig. 2. FEM models of oxygen concentration and islet function under specified culture conditions. (**A**) Simulated oxygen concentration profile after 24 hours of culture in standard static culture compared to continuous perifusion culture in either the Acry-Chip or Oxy-Chip. Islets (outlined in black) are embedded in a hydrogel (outlined in green) and cultured in media (outlined in pink). White regions denote areas of potential dysfunction due to hypoxia ($[O_2]_{dys} \leq 5.1$ μM). (**B**) Quantification of functional islet area, defined as percentage of islet region with an $[O_2] > [O_2]_{dys}$, predicted by FEM models. The violin plots display a five-number summary; statistical analysis by one-way analysis of variance (ANOVA) (Browne-Forsythe and Welch tests corrected for multiple comparisons using Dunnett T3 approach for n = 10; $^{**}P < 0.01$). (**C**) Predicted dGSIS curves for islets after 24 hours of culture within each culture system. The no hypoxia curve represents an ideal insulin secretion profile for healthy islets. Legend at top of graph: [glucose] of the media, G = mM glucose. Insulin secretion is normalized per number of islets (**D**) Predicted total insulin secretion [area under the curve (AUC)] during glucose stimulation from FEM models.

(i.e., dGSIS) further captured culture-induced differences (Fig. 2C). Under ideal culture conditions (no hypoxia control), a classic biphasic dGSIS response curve was predicted, with a first-phase peak insulin release and a second-phase plateau during high glucose stimulation (11 mM), followed by a return-to-baseline secretion levels under non-stimulatory glucose (3 mM) (*22*). While islets cultured in Acry-Chip and Oxy-Chip models were predicted to exhibit no major alterations in this dynamic secretion profile, islets within static cultures were substantially suppressed, with an area under the curve (AUC) during high glucose stimulation of only 67% of the no hypoxia control group (Fig. 2D). Overall, while the additional parameters of islet size and loading density were not explored in this model, FEM generally predicted that continuous perifusion culture within the Oxy-Chip MPS mitigates islet hypoxic stress within the culture niche, resulting in a positive impact on islet health and function compared to static culture conditions.

Rodent islet viability within culture platforms

The accuracy of our computational model predictions was first evaluated via tracking rodent islet viability within alginate hydrogels cultured in static, Acry-Chip MPS, or Oxy-Chip MPS platforms. As seen in the representative live/dead images (Fig. 3A), islets cultured under continuous perifusion in either of the islet MPS platforms qualitatively showed reduced cell death throughout the 3D hydrogel, when compared to islets cultured under static conditions. Quantitative image analysis of live/dead results measured a significantly higher percentage of viable cells in both the Acry-Chip (91.8 ± 7.4%; $P < 0.0001$) and Oxy-Chip (96.3 ± 3.1%; $P < 0.0001$) at 24 hours, when compared to the static control (85.1 ± 11.4%; Fig. 3B). A similar trend in percentage islet viability was observed at 72 hours, although significant differences were not measured between the Acry-Chip and static cultures (Fig. 3C). For both time points, a decreased variance in viability readings was observed for MPS cultures, when compared to static conditions (both $P < 0.0001$, F test). To investigate the potential role of islet isolation effects on these observations, we delineated viability tracking for each of the nine isolations (fig. S3, A to D). While variations in viability across islet batches were measured (fig. S3, A and B), individual isolations exhibited similar trends in viability, as reported for pooled outcomes (fig. S4, C and D). Notably, an increase in islet viability percentage was measured for the static culture group between 24 and 72 hours (fig. S3E), likely due to the natural clearance of dead cells from the culture over time.

Single islet organoid cell death tracking

MPS platforms designed for in situ assessment and tracking provided unique spatiotemporal insight into cellular dynamics. To highlight this versatility in our islet MPS, we tracked the dynamics of cells undergoing apoptosis, as well as those exhibiting either early- or late-stage necrosis, through longitudinal spatiotemporal imaging of specific 3D cellular organoids within the Acry-Chip. This MPS was selected for this study due to the elevated variance in cell death indicated from the live/dead imaging study. For labeling, imaging probes for cellular caspase-3/7–based apoptosis and damaged nuclear DNA were dynamically infused into the circulating media. The Acry-Chip enabled high-content real-time imaging of alginate-embedded rodent islets within sealed culture chambers under continuous flow (movie S1). A representative image series over the course of 3 days illustrated the dynamic changes in the activation of caspase-3/7–based apoptosis within a single primary islet organoid within the Acry-Chip (Fig. 4A). Post hoc image analysis permitted further tracking of these dynamics (Fig. 4B).

Quantification of spatiotemporal changes in apoptosis and cell death over 48 hours of culture revealed distinct differences between static culture and dynamic perifusion culture in the Acry-Chip MPS (Fig. 4, C and D). For apoptotic tracking, two-way analysis of variance (ANOVA) analysis, of the same set of islets with matching factors

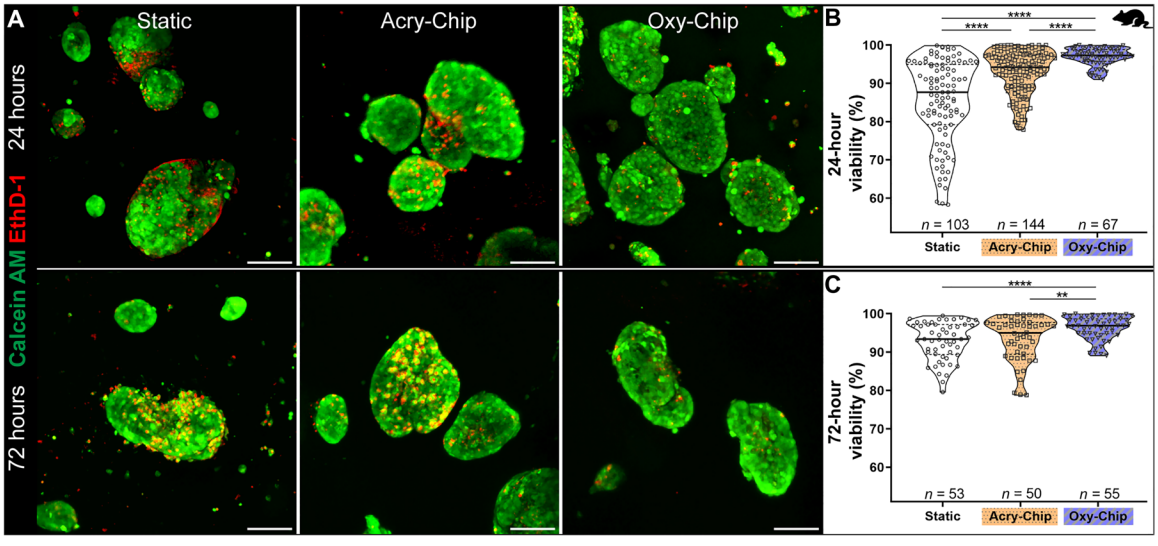

Fig. 3. Hydrogel-embedded rodent islets cultured for 24 and 72 hours in Acry-Chip and Oxy-Chip to evaluate viability. (**A**) Representative live/dead images of islets under all three culture conditions at both 24 and 72 hours. EthD-1, ethidium homodimer-1. Scale bars, 100 μm. (**B** and **C**) Quantitative image analysis of live/dead images after 24 hours (B) and 72 hours (C) of continuous perifusion of islets in all three culture conditions. Viability (%) was calculated as the live cell area divided by the sum of both live and dead cell area of each islet. Statistical analysis by one-way ANOVA [Browne-Forsythe and Welch tests corrected for multiple comparisons using Games-Howell approach for $n \geq 50$ samples; $^{**}P < 0.01$ and $^{****}P < 0.0001$; robust regression and outlier removal (ROUT) test with $Q = 5\%$ to remove outliers]. The violin plots display a five-number summary. Viability quantification results were pooled from more than three independent islet isolations.

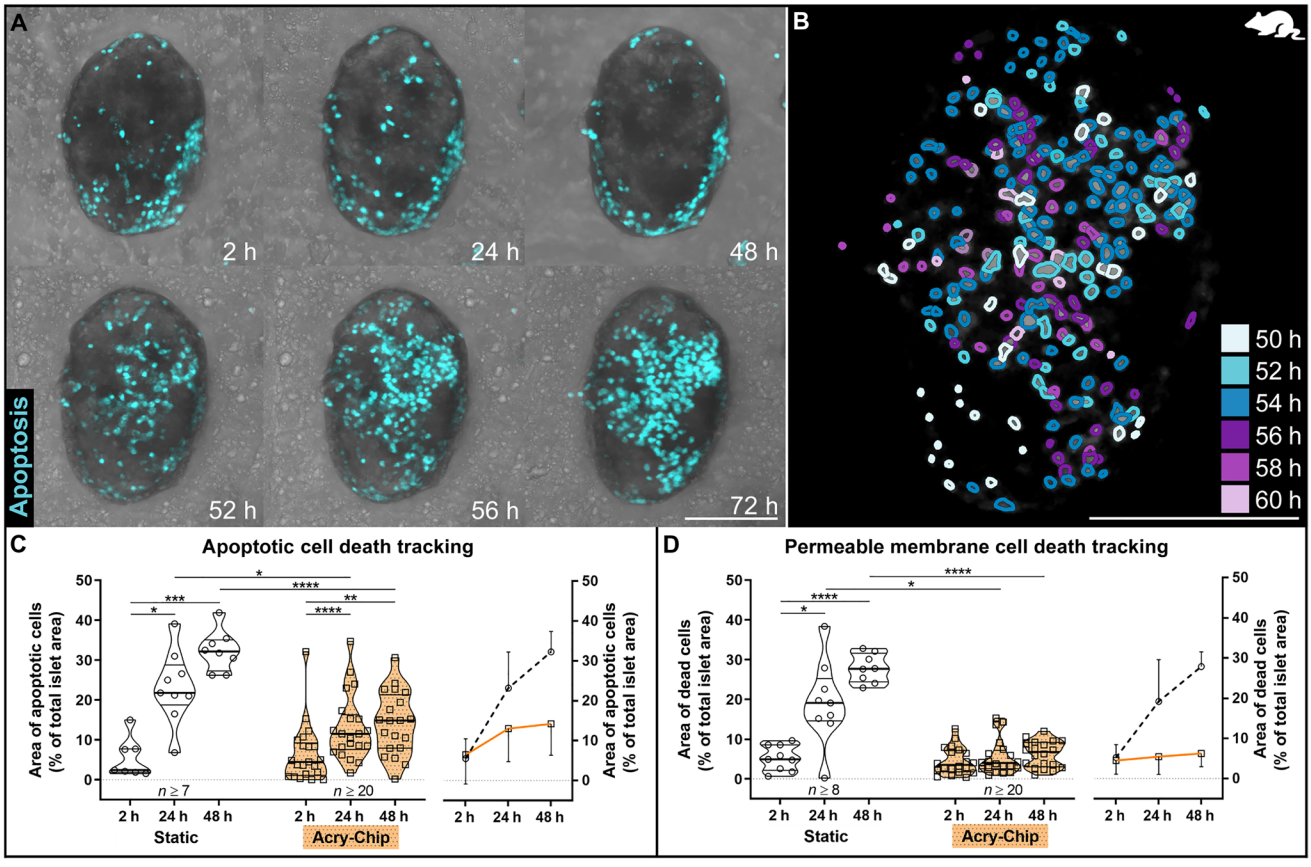

Fig. 4. Temporal cellular death tracking of hydrogel-embedded islets cultured under Acry-Chip or static conditions. (**A**) Time-course snapshots of caspase-3/7–based cell apoptosis (cyan) formation tracked in a single islet organoid continuously cultured in the Acry-Chip for up to 72 hours. Scale bar, 100 μm. (**B**) Tracking accumulation of apoptotic cells in the same islet organoid between 50 and 60 hours, where the apoptosis signal was superimposed and denoted with a color map that corresponds to specific time points. Scale bar, 100 μm. (**C**) Percentage area of apoptotic cells, measured as the percentage area of fluorescence signal from the total designated islet area, was quantified after 2, 24, and 48 hours of culture under Acry-Chip and static conditions. (**D**) Similarly, image quantification for dead cells was acquired from the emitted far-red fluorescence when bound to nucleic acids with permeable membranes at 2, 24, and 48 hours of cultured under both conditions. Statistical analysis by two-way ANOVA with mixed-effects model approach (matching factors; Sidak's multiple comparison to compare between static and Acry-Chip culture conditions, Tukey's multiple comparison to compare time factor within each culture conditions; not assuming sphericity; ROUT test with $Q = 1\%$ to remove outliers; $^{*}P < 0.05$, $^{**}P < 0.01$, $^{***}P < 0.001$, and $^{****}P < 0.0001$). The violin plots display a five-number summary. Quantification results were pooled from three independent assessments.

over time, showed that time and culture platform factors, both independently and combined, have a significant effect on the results ($P < 0.0001$, $P = 0.0012$, and $P < 0.0001$, respectively). For static conditions, a 4.2- and 5.9-fold elevation in the percentage area of apoptotic cells were measured after 24 and 48 hours of culture, respectively, when compared to the initial 2-hour measurement ($P = 0.012$ and $P = 0.0002$, respectively; Fig. 4C and movie S1). Islets cultured in the Acry-Chip initially showed a significant twofold elevation in the percentage of apoptotic cells between culture times 2 and 24 hours ($P < 0.0001$), but this value plateaued by 48 hours. Moreover, at both 24 and 48 hours, the percentage of apoptotic cells within the Acry-Chip was significantly less than for static conditions ($P = 0.034$ and $P < 0.0001$, respectively), demonstrating that the Acry-Chip islet MPS platform mitigated islet cell apoptosis during this culture period. To investigate the potential impact of islet size and cellular death, temporal live-cell tracking results for islets cultured within the Acry-Chip were further delineated into islet size bins and evaluated (fig. S2B). Globally, while there was a significant increase in apoptosis over time across all islet size groups ($P < 0.0001$), islet size was not a contributing factor ($P = 0.958$). Notably, the number of apoptotic cells increased in the Acry-Chip after extended 50 to 60 hours of culture (movie S1).

Tracking accumulated dead cells found that both time and culture platform, either independent or combined, were significant factors ($P < 0.0001$ for all). For static cultures, a significant 3.7- and 5.3-fold increase in the percentage of dead cells within the tracked islets were quantified at 24 and 48 hours, when compared to the 2-hour assessment ($P = 0.011$ and $P < 0.0001$, respectively; Fig. 4D). In stark contrast, the percentage of dead cells within islets cultured in the Acry-Chip remained stable over the entire culture period. At both 24 and 48 hours, a significant 3.5- and 4.4-fold reduction in the percentage of dead cells was measured for islets within the Acry-Chip when compared to the static culture conditions ($P = 0.01$ and $P < 0.0001$). Notably, islet size did not impart a significant effect on the accumulation of dead cells (fig. S2C). Overall, spatiotemporal tracking of cellular changes within the islet MPS was easily measured, with resulting metrics highlighting the beneficial impact of the MPS on islet cell survival.

Monitoring rodent islet function

An advantage of our MPS is the ability to easily perform sequential functional assessments at multiple time points on the same set of organoids. One of the primary endocrine functions of pancreatic islets is to secrete insulin in response to stimulatory glucose levels. A gold-standard assessment to evaluate in vitro islet function is the dGSIS assay, where insulin release in response to dynamic glucose changes is measured with respect to time (Fig. 5A, inset graph). Specific metrics can be obtained from the insulin secretion profile to characterize islet functionality, such as the overall AUC during the glucose challenge, total change in first-phase insulin secretion (Δ), and the rate of insulin release following glucose stimulation (slope). For most dGSIS perifusion systems, recovering the islets after dGSIS is challenging, as islets are either suspended in a slurry of polyacrylamide beads in perifusion chambers or trapped within permanently sealed MPS platforms (*23*, *24*). Hence, dGSIS is typically an end point assay for a single set of islets. Without these restrictions, our MPS permitted sequential glucose challenging of cultured hydrogel-embedded rodent islets at discreet time points (i.e., 24, 72, and 120 hours). Average insulin secretion profiles during dGSIS, aggregated from all isolations and plotted with respect to time, are summarized in Fig. 5A. Islets cultured in either Acry-Chip or Oxy-Chip exhibited robust stimulation profiles in the presence of high glucose, in stark contrast to the minimal responses measured from islets cultured under the static condition for only 24 hours. These differences were more apparent after 72 and 120 hours of culture. While static cultured islets exhibited a complete loss of glucose-stimulated insulin secretion, the Acry-Chip and Oxy-Chip platforms preserved islet functionality for at least 120 hours.

Deeper analysis of dGSIS curves revealed additional differences. Statistical analysis of total insulin secretion, obtained from calculating AUC during high glucose stimulation, found the culture platform to impart a significant effect ($P \leq 0.0001$, two-way ANOVA; Fig. 5B). The AUC for islets was significantly elevated within the Acry-Chip and Oxy-Chip, at 34.2- and 36.6-fold higher than static culture controls after 24 hours (both $P \leq 0.0001$; Fig. 5B). After 72 hours, similar trends were observed, with the total insulin secretion of islets cultured under Acry-Chip and Oxy-Chip quantified as 47.5- and 60.7-fold higher than static culture ($P = 0.0001$ and $P \leq 0.0001$, respectively). Comparison of time effects across culture platforms found no

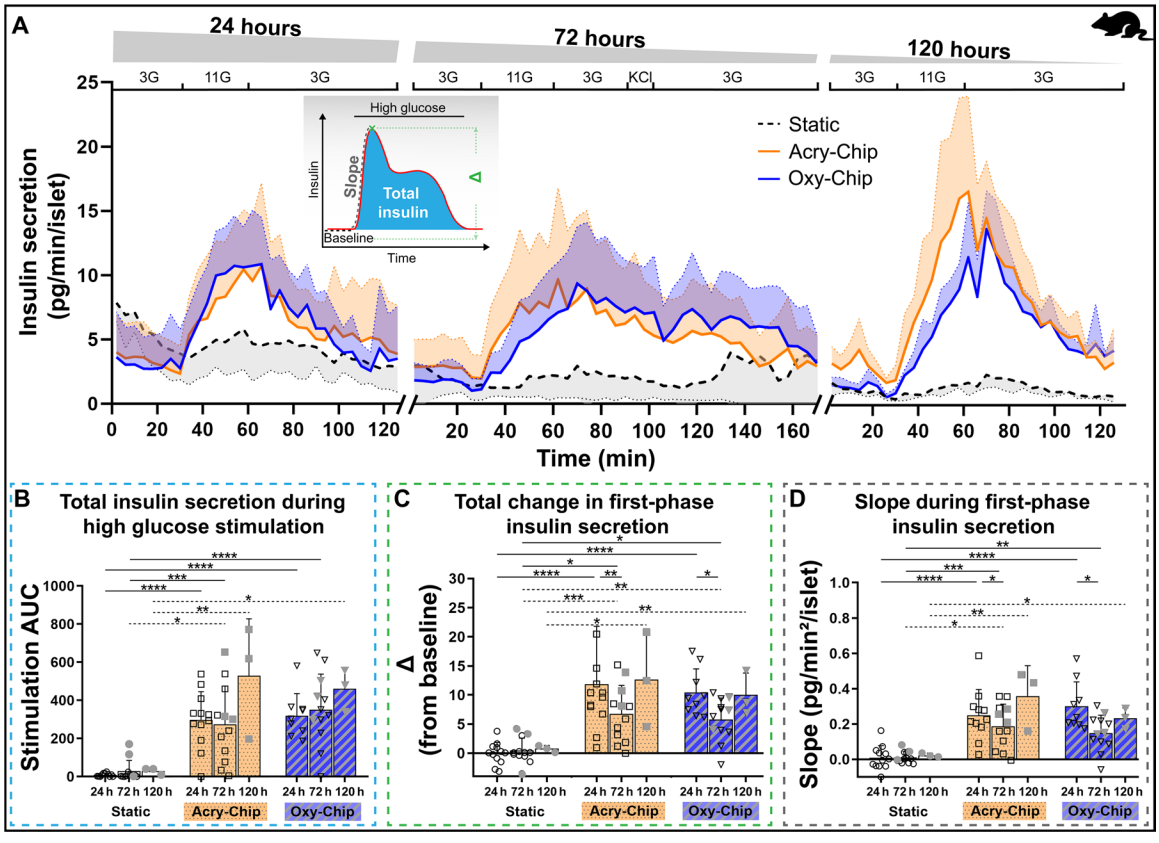

Fig. 5. Serial functional assessment of hydrogel-embedded rodent islets cultured under MPS or static conditions. (**A**) dGSIS profiles of same sets of islets over time (one isolation was evaluated at 72 and 120 hours). The shaded area of the dGSIS profiles represent SD values corresponding to its means. Legend at top of graph: [glucose] of the media, G = mM glucose. Inset graph: Idealized dGSIS profile identifying the origin of different matrices. (**B**) Calculated AUC representing total insulin secretion during high glucose stimulation peak. (**C**) Total change between maximum insulin secreted and its respective average baseline during glucose challenge. (**D**) Slope of the dGSIS profile between the last baseline value and maximum insulin secreted during glucose challenge. (B to D) Statistical analysis of 24 and 72 hours by two-way ANOVA with mixed-effects model approach (matching factors; Sidak's test to compare between culture conditions; Tukey's test to compare time factor; assumed sphericity; ROUT test with $Q = 1\%$ to remove outliers; $^{*}P < 0.05$, $^{**}P < 0.01$, $^{***}P < 0.001$, and $^{****}P < 0.0001$). Data points extracted from a single batch assessed at 72 and 120 hours are color coded in gray with distinct statistical analysis depicted via dashed lines. dGSIS profiles at 24 and 72 hours are from more than three rodent islet isolations with $n \geq 9$ biological replicates. dGSIS profiles at 120 hours are from a single-rodent islet isolation with $n = 3$ biological replicates.

significant changes, indicating stability in function over time, regardless of the culture platform. AUC assessed separately for the rat isolation sequentially evaluated at 72 and 120 hours showed similar trends (Fig. 5B, only gray data points and its statistics depicted with dashed lines). The change in first-phase insulin secretion (Δ) was also significantly affected by both the culture platform and the duration of culture ($P < 0.0001$ and $P = 0.002$, respectively, two-way ANOVA; Fig. 5C), with islets cultured in both Acry-Chip and Oxy-Chip expressing elevated Δ when compared to the static control. Similar trends were observed for Δ values measured from the isolation evaluated at 72 and 120 hours (Fig. 5C, gray data points). The efficiency of the islet's functional response to glucose challenge, captured by the dGSIS slope following exposure to stimulatory glucose levels, was also significantly affected by both the culture platform and time ($P \leq 0.0001$ and $P = 0.008$, respectively, two-way ANOVA; Fig. 5D). Islets cultured under static conditions were nonresponsive to the high glucose challenge, resulting in a close-to-zero average slope values (0.009 ± 0.068 and 0.011 ± 0.033 pg/min^2/islet at 24 and 72 hours, respectively), in stark contrast to islets cultured in Acry-Chip and Oxy-Chip ($P \leq 0.001$ for both islet MPS at 24 hours and $P = 0.001$ and $P = 0.009$, respectively, at 72 hours). Singularly assessed slope values for 120 hours showed 15.8- and 10.3-fold elevation for Acry-Chip and Oxy-Chip, respectively, when compared to the static culture conditions ($P = 0.001$ and $P = 0.03$, respectively; Fig. 5D, gray data points). These results highlight the ability of our islet MPS to retain robust and efficient islets' responsiveness to glucose challenges throughout the culture duration.

Additional functional assessment of alginate-embedded rodent islets cultured within the islet MPS was performed via multiplex hormonal measurement of dGSIS analytes collected at the 24-hour time point (fig. S4). The secretion of α cell hormones glucagon and glucagon-like peptide-1 (GLP-1) was suppressed when glucose levels were switched from low to high for all culture conditions, indicating functional α cells within the pancreatic islet (fig. S4, A and B). Contrarily, supplementary hormones of healthy β cells, specifically C-peptide and amylin, showed dysfunction in static cultures, with no elevated secretion during the high glucose challenge (fig. S4, C and D). For islets cultured in Acry-Chip, however, a significant stimulatory response to the glucose challenge was observed for both C-peptide and amylin. Oxy-Chip cultures only exhibited a significant change in amylin. These results support the early dysfunction of β cells within the suboptimal static culture, with limited impacts on α cell functionality.

Characterizing benefits of MPS for human islet culture

Translating this work to human cell sources, the in vitro function of nondiabetic human islets was characterized. Alginate-embedded human islets were perifused in the Acry-Chip or Oxy-Chip MPS or cultured under standard static conditions for up to 10 days, with functional assessments performed at 24, 48, 72, and 240 hours. Results from two separate islet isolations are summarized in Fig. 6 and fig. S5. In general, human islets cultured in 3D alginate hydrogels under static conditions exhibited a nonresponsive glucose stimulation profile during the testing window (Fig. 6A and fig. S5A), resulting in removal of this group after 72 hours. Conversely, human islets cultured within either the Acry-Chip and Oxy-Chip exhibited highly functional islets over the entire culture window (Fig. 6A and fig. S5A). For one preparation, extended culture within the MPS resulted in significant improvements in islet functionality, with significant improvements in total insulin secretion (Fig. 6B), net insulin release in first phase (Fig. 6C), and functional efficiency (Fig. 6D) over the culture time ($P < 0.001$, $P < 0.0003$, and $P < 0.003$, respectively, two-way ANOVA). Extending the culture window to 240 hours resulted in no measurable declines in human islet function, as characterized by dGSIS. Furthermore, the Acry-Chip and Oxy-Chip systems supported the functional islets in a statistically equivalent manner during the 240-hour culture window. Similar trends in robust insulin responses for islets cultured in the MPS were observed for the other human islet preparation (fig. S5, B to E). With a highly robust insulin response measured for islets within the Oxy-Chip at 24 hours, overall dGSIS metrics (AUC, Δ, and slope) remained stable during the culture window. Collectively, despite a rapid loss in function under static conditions, the functional output of human islet organoids encapsulated in a 3D matrix was highly preserved during extended in vitro cultures within both the Acry-Chip and Oxy-Chip MPS platforms.

In situ interrogation of β cell glucolipotoxicity

After establishing the suitability of these MPS for extended islet organoid culture, we sought to demonstrate how this platform can provide unique physiological insight into the impacts of discrete stimuli on organoid phenotype and survival. For example, it is known that type 2 diabetes emerges from the long-term exposure of β cells to hyperglycemic and hyperlipidemic conditions (*25*–*27*). Ex vivo interrogation into the role of glucose and lipid concentration and duration on subsequent β cell dysfunction and toxicity, however, is typically limited to assessment at discrete time points after static exposure. The replacement of standard culture dishes with our MPS platform permits in situ, temporal, and live cell assessment of the dynamic glucolipotoxic impact on the pancreatic islet.

Rodent islets were transduced with calcium biosensor (GCaMP6m) to track changes in intracellular Ca^{2+}, a surrogate marker for insulin secretion from β cells, in response to toxic conditions (*22*, *28*). Following viral infection, pancreatic islets were embedded in alginate hydrogels and loaded into two independent channels within the Acry-Chip (Fig. 7A). Continuous time-lapse confocal images captured changes in intracellular Ca^{2+} (Fig. 7B, i) and cell death (Fig. 7B, ii) in response to dynamically perifused stimuli (movie S2). As summarized in Fig. 7C, each MPS channel was first exposed to a glucose challenge, followed by 2.5 hours of culture in basal or glucolipotoxic media. The initial high glucose challenge validated time-lapse imaging of the Ca^{2+} sensor as a measure of islet functionality [Fig. 7, B (i) and D, and fig. S6], with hydrogel-embedded islets exhibiting robust Ca^{2+} in response to high glucose, followed by a return-to-baseline intracellular Ca^{2+} levels under nonstimulatory glucose. Quantification of stimulatory profiles via AUC found statistically equivalent responses between both channels [channel 1 (Ch1), AUC = 27.0 a.u. (arbitrary units) × min; Ch2, AUC = 27.5 a.u. × min; $P = 0.2099$). It also identified glucose-responsive β cells for temporal tracking. Following a 70-min recovery period under basal media, Ch1 islets were perifused with glucolipotoxic media of high glucose (16.7 mM) and sodium palmitate (500 μM) for 2.5 hours. Post hoc analysis of resulting Ca^{2+} signaling traces revealed hyperresponses from β cells perifused with high glucose and fatty acid, when compared to traces obtained from other β cells exposed to basal glucose media (Fig. 7E and fig. S6). Quantification of Ca^{2+} AUC during the treatment window found significantly elevated levels for treated versus control β cells ($P = 0.0004$; Fig. 7F). Tracking of accumulated dead cells over the treatment window implicated β cell

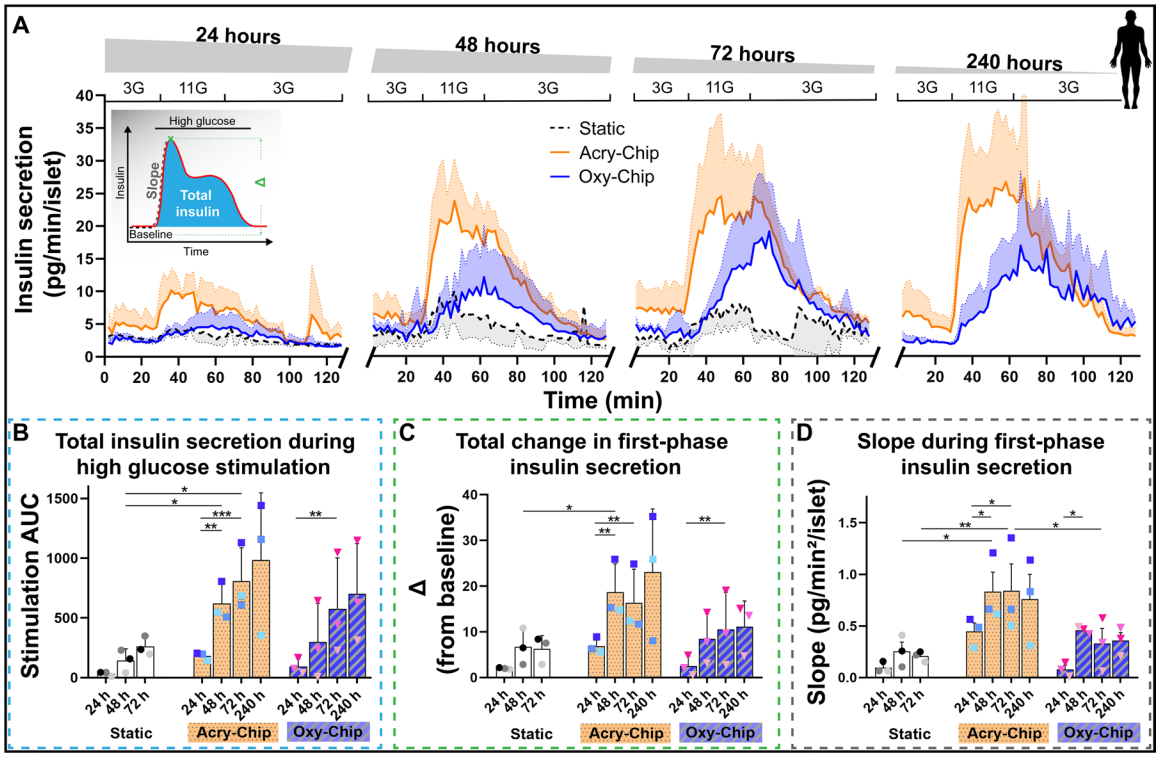

Fig. 6. Serial functional assessment of human islets embedded with hydrogels and cultured in Acry-Chip or Oxy-Chip MPS for up to 240 hours. (**A**) Serial dGSIS assessment of human islets cultured under islet MPS and static condition at 24, 48, 72, and 240 hours. The shaded area of the dGSIS profiles represent SD values corresponding to its means. Legend at top of graph: [glucose] of the media, G = mM glucose. The inset graph shows an idealized dGSIS profile identifying the origin of different matrices. (**B**) Calculated AUC representing total insulin secretion during high glucose stimulation peak. (**C**) Total change between maximum insulin secreted and its respective average baseline during high glucose challenge. (**D**) Slope of the dGSIS profile between the last baseline value and maximum insulin secreted in response to the high glucose challenge. (B to D) Data points are depicted in color pallets to visually track biological replicates over time. Statistical analysis by two-way ANOVA with repeated-measures approach (matching factors; Tukey's multiple comparison to compare between static, Acry-Chip, and Oxy-Chip culture conditions; Tukey's multiple comparison to compare time factor within each culture conditions; assumed sphericity; $*P < 0.05$, $**P < 0.01$, and $***P < 0.001$). Statistical analysis for 240 hours was performed by unpaired *t* test with Welch's correction. dGSIS profiles are from a single islet isolation batch preparation with $n = 3$ biological replicates.

toxicity in response to the glucolipotoxic treatment, with a 1.8-fold increase in dead cell area for islets exposed to treatment, when compared to the same islets at the beginning of the experiment ($P = 0.018$). Contrarily, islets cultured under basal conditions did not exhibit significant changes in cell death over the same culture time. In general, these results highlight that our islet MPS can perform in situ Ca^{2+} imaging at sufficient resolution to feasibly track and quantify how organoids embedded in 3D hydrogels respond to toxic stimuli within a dynamic microenvironment.

DISCUSSION

Our MPS platforms, both the Acry-Chip and Oxy-Chip, supported the prolonged survival of perifused 3D organoids within hydrogel matrices, while also permitting ease in longitudinal (serial) imaging and functional cellular assessments. Replacing the commonly used PDMS with PMMA as the base fabrication material avoided many of the critical challenges faced in using PDMS-MPS for drug screening or long-term organoid culture, such as problems with accurate large-scale manufacturing and biofouling (*29*, *30*). While others have also made this transition using polycarbonate (*31*), long-term microfluidic culture using plastic-based MPS is challenged by the poor oxygen permeability of these materials (*32*). We address this issue by integrating a PFA membrane, an oxygen-permeable and low biofouling perfluorinated polymer, into the acrylic MPS platform (*33*). The PFA membrane facilitates oxygen transport at the cell culture niche, while retention of PMMA as the primary fabrication material ensures a robust and stable framework suitable for large-scale manufacturing.

Following isolation, multicellular islet organoids cultured under static culture exhibit temporal declines in β cell function, endothelial cell loss and coalescence, and elevated cell death, restricting their utility in pharmaceutical and physiological studies (*5*, *34*). Here, primary islet organoids were leveraged as an effective model to demonstrate the utility of our MPS, as controlled and dynamic perifusion of islet organoids in culture serves to replicate their highly perfused native microenvironment. FEM models, which coupled pancreatic islet physiology and mass transport, predicted reduced hypoxic stress and enhanced insulin secretion for islets within the Acry-Chip and Oxy-Chip platforms when compared to static cultures; these expectations are in line with previous correlations between oxygen availability and islet function (*17*, *35*, *36*).

In vitro tracking of islet viability largely correlated with FEM models, although some variation across the three platforms was evident. This variance can be attributed to the differences in islet isolation batches, as each islet isolation procedure is subjected to differences

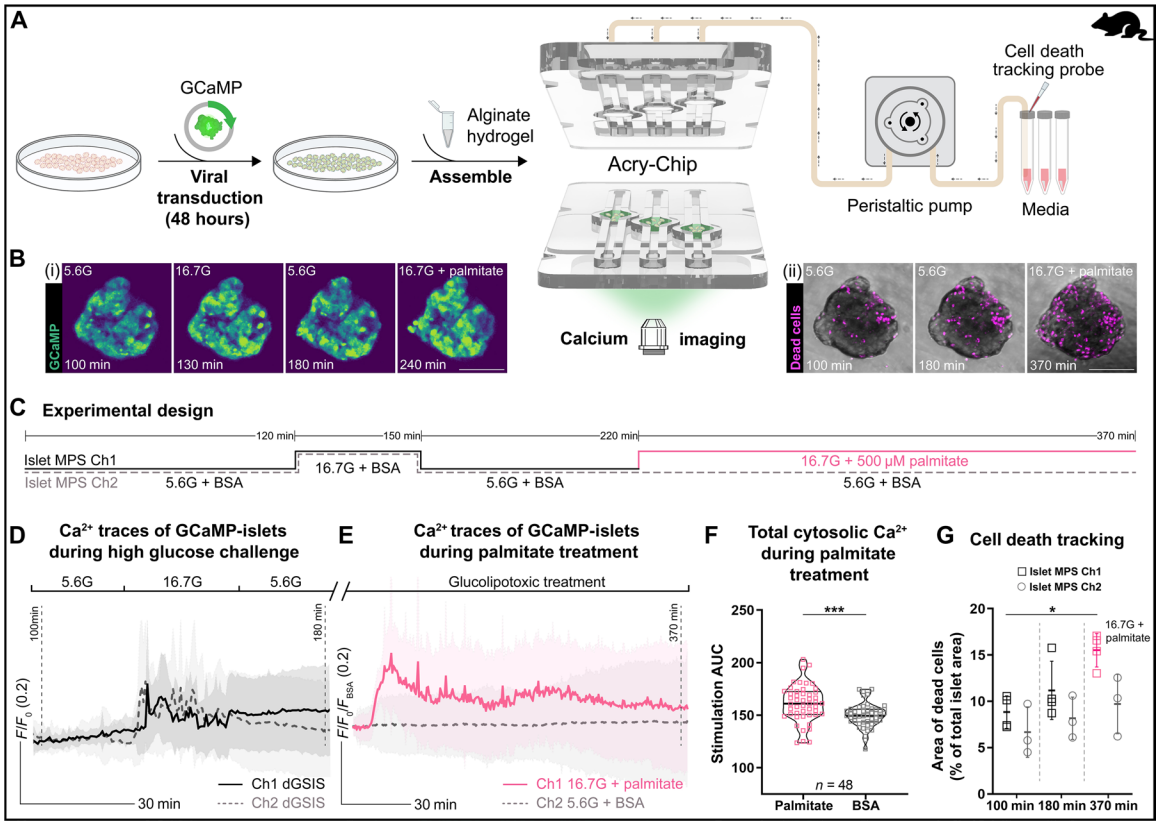

Fig. 7. Interrogation of glucolipotoxicity stimuli on in situ Ca^{2+} signaling and viability of hydrogel-embedded pancreatic islets within Acry-Chip via longitudinal confocal imaging. (**A**) Schematic representation of experimental workflow. (**B**) Time-course snapshots of a representative (i) GCaMP islet and (ii) accumulated dead cells when exposed to designated concentration of glucose and glucolipotoxic agent. Scale bars, 100 µm. (**C**) Schematic representation of the experimental design for the toxicity study illustrating different media compositions and channels with its respective exposure time. Notably, the time stamp is not drawn to scale. G = mM glucose. (**D**) Ca^{2+} signaling traces for islets within the two different designated channels of the Acry-Chip during the time-step glucose challenge. (**E**) Ca^{2+} traces for islets cultured in glucolipotoxic media. Notably, traces were further normalized to average Ch2 bovine serum albumin (BSA) traces to highlight signal changes between channels. (**F**) Calculated AUC representing total cytosolic Ca^{2+} during toxicity treatment. (**G**) Percentage area of dead cells within specific islets quantified at the beginning of both the experiment (100 min) and toxicity treatment (180 min), and at the end of the treatment (370 min). Statistical analysis for AUC by unpaired *t* test with Welch's correction (***$P < 0.001$; ROUT test with $Q = 1\%$ to remove outliers) and for death tracking by one-way ANOVA (Browne-Forsythe and Welch tests corrected for multiple comparisons using Dunnett T3 approach for $n < 50$; *$P < 0.05$). Ca^{2+} traces are from a single-rodent islet isolation batch preparation.

in each pancreatic digestion times, enzyme batches, human errors, etc. While this batch-to-batch inconsistency is expected, note that it did not affect global interpretations. Variability in islet sizes, which can range from as low as 50 µm to as high as 400 µm in diameter, can also alter responses, as increased islet size can exacerbate intra-islet nutritional gradients and elevate central necrosis in larger islets (*37*, *38*). For our assessments, we did not observe correlations between islet diameter and cell apoptosis or necrosis for islet cultured within the Acry-Chip. While this may be due to improved nutritional gradients resulting from convective transport, we are cautious in overinterpretation of these results, as depth restrictions in confocal imaging skews image analysis to the organoid periphery, which can potentially underestimate global changes. Last, imaging of cell death is a dynamic event; thus, temporal clearance of dead cells leads to loss of necrotic signaling over time. Despite these factors, live/dead imaging demonstrated significant benefits of both the Acry-Chip and Oxy-Chip platforms over the initial 72-hour testing period, when compared to static cultures. The increased variability of viability for static cultures also correlated with computational models of hypoxic stress. Overall, the dynamic culture of hydrogel-embedded islets within our MPS resulted in an improved maintenance of islet viability, with enhanced consistency of this metric for up to 72 hours.

Our MPS platforms also supported imaging at a sufficient resolution for spatiotemporal tracking of single cells within a given islet organoid. Temporal visualization of cells undergoing caspase-3/7–based apoptosis traced the preferential emergence of apoptotic cells at the organoid periphery, regardless of the culture platform. This pattern of peripheral cell loss was expected, as detachment-induced apoptotic cell death (i.e., anoikis) early in islet culture is well documented (*39*–*41*). While encapsulation of islets within hydrogels can serve to mitigate this effect via recapitulation of integrin and cadherin anchors at the islet border, the alginate matrix used in this study lacks cell recognition sites and extracellular matrix (ECM) cues (*42*). Thus, future studies combining ligand-functionalized alginate or decellularized ECM hydrogels and genetically encoded fluorescent cellular identifiers can be designed to further characterize and mitigate anoikis (*43*, *44*).

Despite being encapsulated with the same inert matrix, statically cultured alginate-embedded islets exhibited significant and early elevations in the number of apoptotic and terminally necrotic cells,

when compared to MPS cultured islets. This trend is likely a result of dynamic flow, which improved nutrient delivery; however, the observation that elevated apoptosis was observed at the periphery of the organoid, where nutrient delivery is less deficient, indicates that continuous islet perifusion may instigate other effects. Biomechanical stress induced by laminar flow has been reported to alleviate endothelial cell apoptosis and promote vascularization of organoids (*45*). Thus, it is possible that continuous tensional forces exerted on transmembrane integrin receptors lead to balancing of dynamic forces that consequently govern intracellular apoptotic processes. Although postulations have been made regarding the physical forces within the pancreatic islet microenvironment, the specifics of in vivo islet shear stress are largely unknown (*46*). Within the geometry of our platform, a flow rate of 30 μl/min, which imparted and estimated an average fluid shear stress of 0.27 dynes/cm^2 at the boundary of the islet regions, supported extended culture without imparting dysfunction. While further investigation on the role of shear stress in maintaining islet function is warranted, the use of bioimage informatics analysis demonstrates the capability of the platform for high-content imaging of longitudinal spatiotemporal changes for assessing the health of cells in a continuously dynamic microenvironment. The establishment of these features permits future temporal investigation into factors that can enhance or stabilize organoid cell culture.

Islet functional assessments correlated well with spatiotemporal imaging observations. Statically cultured human and rodent hydrogel-embedded islets exhibited nonfunctional insulin release profiles after only overnight culture. This precipitous loss of function is attributed to significant oxygen deprivation, as well as apoptotic-induced islet dysfunction, and highlights the challenges of culturing these primary organoids within 3D hydrogels using conventional culture systems (*47*). In stark contrast, our MPS platform retained robust glucose-stimulated insulin secretion for both human and rat islets for at least 5 to 10 days. Further investigation into rodent dGSIS profiles during MPS culture did exhibit some features divergent from an ideal stimulatory trace. For example, a classic biphasic insulin secretion profile was not observed for rodent islets. This is likely due to the combination of insufficiently stimulatory glucose levels, blunting of the first-phase response due to the additional flow barrier imposed by the hydrogel, and the 3- to 30-fold lower perifusion rates used during this dGSIS study (*15*, *23*, *35*, *48*, *49*). Furthermore, after 72 hours of continuous culture, rodent islet insulin secretion after high glucose stimulation did not fully return to its original baseline levels. This feature indicates early islet stress due to ionic channel leakage or accumulated reactive oxygen species (ROS) (*50*, *51*). Thus, future studies will identify the ideal glucose levels and flow rates needed to optimize effluent insulin release, as well as explore other hydrogels that may decrease any biomaterial-induced dampening. Islet culture media will also be screened, as recent work indicates that this plays a considerable role in long-term ex vivo islet survival (*52*). All of these features are easily manipulated in the islet MPS due to the modularity of its workflow.

Both MPS platforms were highly supportive of long-term human pancreatic islet culture and serial characterization. Ease in sequential organoid evaluation permitted detailed tracking of functional trends, clearly demonstrating that the MPS provides an islet-supportive environment. Specifically, one islet preparation displayed robust functionality throughout the assessment period, while the other exhibited improved and then stable insulin response indices over the 10-day culture period. Classic single time-point dGSIS measurements could not have delineated these trends. With ease in temporal functional monitoring, human islets studies can now explore the potential of islets to recover from insults associated with isolation, transport, and/or manipulation, as well as investigate the transient impacts of various pharmaceuticals.

For both human and rat islets, no significant difference in islet function was observed between the two MPS platforms, despite models predicting a modest impact of the oxygen-permeable membrane on insulin secretion during high glucose stimulation under these experimental conditions. This discrepancy is likely due to the optimized flow rates used for this system, as others have reported benefits in the inclusion of oxygen-permeable membranes for the static culture of organoids or tissues (*53*–*55*). At this transport scale, the inclusion of convective forces will dominate diffusive contributions; thus, the addition of enhanced oxygen diffusion within the culture niche will be less beneficial when the system is under a continuous flow field. Hence, the more easily manufactured AcryChip system provides optimal nutritional support for long-term culture of complex human and rodent pancreatic islet organoids. However, for culture conditions where high organoid densities are used, the use of the Oxy-Chip system may modulate detrimental oxygen gradients.

The utility of the islet MPS for pathophysiological modeling was illustrated by performing a glucolipotoxicity study. It is well documented that the exposure of β cells to lipids, such as free fatty acids (FFAs), induces concentration and time-dependent alterations in viability and functionality (*56*–*58*). While physiological plasma levels of FFAs, generally between 200 and 600 μM in healthy adults, can exert positive effects on the function of β cells, long-term exposure can lead to β cell dysfunction and toxicity (*59*, *60*). Exposure to hyperglycemic treatment can further exacerbate detrimental effects (*61*, *62*). While 1 to 3 days of exposure to FFAs increases the production of ROS generation, endoplasmic reticulum stress, abrupt cytosolic Ca^{2+} signaling, and eventually cell death, our results indicate that a treatment window as little as 2.5 hours can elevate cell death (*57*, *58*, *60*, *63*). While we are cautious in drawing conclusions of the exact mechanism at play here, the results clearly demonstrate the utility of our islet MPS to perform in situ β cell–specific tracking of cytosolic Ca^{2+} signaling and correlate cell death in the absence and presence of a dynamic glucolipotoxic stimuli. Future studies can use the MPS to fully interrogate the role of hyperglycemic and hyperlipidemic conditions on β cells, providing further insight into the pathogenesis of type 2 diabetes.

Overall, the MPS platforms described herein provide a distinct portfolio of capabilities not available in other platforms, specifically long-term culture, controlled and dynamic perifusion, in situ imaging, serial cell assessments during extended culture, and ease of sample retrieval. Acute multimodal characterization of islets has been reported, but devices used lack long-term culture capabilities and ease in unsealing the device for terminal assessments (*23*, *49*). Complex platforms, such as the Mimetas OrganoPlate, supports 3D cell culture within hydrogel matrices and assessment via optical assays, but their passive perifusion mechanism limits dynamic secretion assays (*64*–*66*). The TissUse two-organ chip couples pancreatic islet microtissues and liver organoids (*67*); however, functional assessment of islets was performed off-chip, and the system did not include a 3D hydrogel matrix. Our platform is limited by its three-channel form factor and the need for off-line functional assessment [such as enzyme-linked immunosorbent assay (ELISA) assays]; future platform

development will be focused on expanding throughput and in situ functional assessment without sacrificing ease in usability.

This study highlights the capacity of our islet MPS to elucidate complex islet physiological and pathophysiologic processes by combining dynamic 3D culture, optical assessment, and functional assays. Moreover, this MPS platform can be used to study temporal interactions between complex matrices and other 3D organoids, while also limiting the amount of sample required for assessment. Ultimately, the culture and multiparametric assessment of organoids in this MPS may provide valuable data for the development of emerging therapeutics and the study of diabetes.

MATERIALS AND METHODS

Design and fabrication of the organoid MPS

The design of the modified fluidic chips was performed in SOLIDWORKS 2018 3D CAD software (Dassault Systèmes, France). Fluidic chips were machined from optically clear PMMA workpieces (McMaster-Carr, Elmhurst, IL) using an MDX-540 CNC milling machine (Roland, Japan). The final form factor of the fluidic chip was laser-cut from the workpiece with a 30-W CO_2 laser engraver (Epilog Laser, Golden, CO). To locally supply oxygen to islets, the culture wells were through cut, and a 25-μm-thick PFA membrane (McMaster-Carr, Elmhurst, IL) was bonded to the bottom piece of the device using a silicone adhesive (McMaster-Carr, Elmhurst, IL). The fluidic device was assembled in a commercially available microfluidic chip holder (Micronit Microfluidics, The Netherlands) with silicone gaskets, developed in-house, to seal the system and introduce fluidic connections. To prevent bubbles from entering the fluidic chip, a low-volume bubble trap (Darwin Microfluidics, France) was placed in the fluid line just before the inlet. The fluidic devices were sterilized with ethylene oxide gas before the cell culture experiments.

Oxygen partial pressure measurement

To measure oxygen in the fluidic platform, an optical oxygen sensor was incorporated into the fluidic chip. Briefly, an oxygen spot sensor was bonded to the roof of the culture well, and the partial pressure of oxygen was monitored via polymer optical fibers connected to a multichannel oxygen meter (PreSens, Germany). The fluidic platform was first purged of oxygen by pumping in nitrogen. Once the oxygen pressure was sufficiently low, the nitrogen flow was shut off, and the partial pressure of oxygen was recorded for 5 min, while oxygen from the ambient air permeated into the culture well. Oxygen permeation measurements were performed at room temperature.

Computational modeling

FEM models of fluid dynamics, mass transport, and rodent pancreatic islet function within the MPS was developed in COMSOL Multiphysics 5.0 (COMSOL Inc., Burlington, MA). The model consisted of a 2D cross section of the islet MPS geometry and 10 circular regions, each representing an islet with a diameter of 150 μm, spaced 750 μm apart. A static culture model was developed on the basis of the geometry of a single well from a 48-well culture plate. Both the islet MPS and static culture models included an alginate region. Fluid dynamics were governed by the incompressible Navier-Stokes equation with a no-slip boundary condition. Convective and diffusive mass transports of oxygen, glucose, and insulin were governed by the generic equations in the Chemical Species Transport Module of COMSOL. Diffusion coefficients for each species in different media were obtained from literature (*35*). Islet function was incorporated using a previously described and validated local concentration-based insulin secretion model (*15*). Hypoxia-induced islet dysfunction was defined as the islet area where oxygen concentration was below 5.1×10^{-4} mol/m^3 after simulating 24 hours in culture. Insulin secretion from islets in the static culture model was determined by recreating the dysfunctional area in a dGSIS model within the Acry-Chip geometry. All parameters used for the present model are summarized in table S1.

Pancreatic islet isolation and culture

All animal procedures were conducted under Institutional Animal Care and Use Committee–approved protocols at the University of Florida and in accordance with the National Institute of Health guidelines. Rodent islet isolations were performed on 250 to 280 g of male Lewis rats (Envigo, United Kingdom), using methods described previously (*68*). The widely accepted technique of handpicking islets was used for experiments, and the histogram of size distribution is shown in fig. S2A. This approach also allowed us to reliably normalize hydrogel-embedded organoids for functional assessments without affecting the islets during postprocessing treatment(s). Human islets were obtained either from the National Institute of Diabetes and Digestive and Kidney Diseases (NIDDK)–funded Integrated Islet Distribution Program (IIDP) or the Human Islet Cell Processing Facility at the Diabetes Research Institute (University of Miami Miller School of Medicine, Miami, FL). The reported human islets data were generated from a nondiabetic female donor [weight, 82 kg; body mass index (BMI), 32 kg/m^2; IIDP Research Resource Identifier (RRID), SAMN08612554] and a nondiabetic male donor [weight, 92.5 kg; BMI, 27.6 kg/m^2; United Network for Organ Sharing (UNOS) no., AHCH197]. Human islets were obtained within 6 days after isolation from isolation center at the University of Miami at the islet viability and purity of 90%. Both human and rodent islets were cultured in CMRL-1066–based media (Mediatech, Manassas, VA) supplemented with 10% fetal bovine serum (HyClone Laboratories, Logan, UT), 25 mM HEPES, 2 mM L-glutamine, and 1% penicillin-streptomycin (all from Sigma-Aldrich, St. Louis, MO) under standard incubator culture conditions (37°C, 5% CO_2). Rodent islets after isolation and human islets after receiving were cultured overnight in 100 mm by 15 mm nontissue-culture petri dish(es) at the loading density of 120 IEQ/cm^2 within media of approximately 1.3 mm in height before utilization for each experiment.

Islet encapsulation and culture

Ultrapure, cyclic guanosine monophosphate–grade, medium viscosity sodium alginate [Novamatrix PRONOVA UP MVG; molecular weight, >200 kDa; guluronic acid/mannuronic acid ratio, ≥1.5; DuPont, Norway] was dissolved at 1.6% (w/v) in sterile 1× phosphate-buffered saline (PBS) and filtered through 0.22-μm nylon syringe filter. Islets were handpicked and embedded in prepared alginate, at a loading density of 50 to 100 islets per 25 μl of alginate precursor solution, by gentle mixing until islets were homogeneously distributed within the matrix. The uncrosslinked islet-alginate mixture was then transferred to a standard 48-well plate or loaded within an Acry-Chip or Oxy-Chip cell culture well. Alginate was then gelled via 10-min exposure to $BaCl_2$-MOPS buffer [50 mM $BaCl_2$, 10 mM MOPS, 3 mM KCl, 50 mM NaCl, and 0.2 mM Tween 20 (pH 7.4)], followed by three washes with sterile 1× PBS. Islet MPS were then assembled, as described above. Notably, islet cell density was kept

consistent for all experiments reported herein. During long-term experiments, islets within the islet MPS were continuously perifused with media at a constant flow rate of 30 μl/min. Static control samples were cultured in a nontissue-culture 48-well plate and incubated with 150-μl media, thus keeping a consistent media height across all platforms. Culture media for all experiments was refreshed every 48 hours.

Immunofluorescence staining

Live/dead staining was performed using the LIVE/DEAD Viability/Cytotoxicity Kit for mammalian cells (Thermo Fisher Scientific, Waltham, MA). Briefly, live cells were distinguished by the presence of intracellular esterase activity, detected by enzymatic conversion of nonfluorescent cell-permeant dye calcein acetoxymethyl (AM) to fluorescent calcein retained in live cells [excitation/emission (ex/em), ~494/~517 nm]. Dead cells were distinguished by ethidium homodimer-1 entering the cells with damaged membranes, where it undergoes a 40-fold enhancement of fluorescence after binding to nucleic acids (ex/em, ~528/~617 nm). Calcein AM (2 μM) and ethidium homodimer-1 (4 μM) were added to individual islet MPS wells for at least 90 min under standard incubator culture conditions (37°C, 5% CO_2). For spatiotemporal time-course experiments, cells undergoing apoptosis and dead cells with a permeable cell membrane were tracked using CellEvent Caspase-3/7 Green ReadyProbes (2 drops/ml) and NucRed Dead 647 ReadyProbes reagents (2 drops/ml) (all from Thermo Fisher Scientific, Waltham, MA). The probe to detect early apoptosis is a four amino acid peptide (DEVD) conjugated to a nonfluorescent nucleic acid–binding dye. This probe upon activation of intracellular caspase-3/7 pathway cleaves the DEVD peptide, allowing the nucleic acid–binding dye to bind to DNA and fluoresce in live cells (ex/em, ~502/~530 nm). Dead cells were distinguished using a live-cell impermeable dye that emits bright far-red fluorescence when bound to nucleic acids in cells with permeable membranes, similar to propidium iodide (ex/em, ~642/~661 nm). For imaging live cells, a temperature and gas chamber–controlled microscope enclosure (Okolab, Italy) was used to maintain standard incubator culture conditions (37°C, 5% CO_2). The imaging probes were fused in the islet culture media, continuously recirculated, and kept within the microscope enclosure for the entirety of the experiment.

Confocal microscopy and image analysis

Imaging was performed using a Leica TCS SP8 confocal microscope (Leica Microsystems, Germany) with HC PL FLUOTAR 5×/0.15 NA (numerical aperture), HC PL APO CS2 10×/0.40 NA, and HC PL FLUOTAR L 20×/0.40 NA air objectives. Cell viability and spatiotemporal time-course images were acquired at 1024 × 1024 pixel resolution. Calcium imaging was acquired at 512 × 512 pixel resolution at 30-s intervals between each cycle. Most image analysis and quantifications were performed in ImageJ (National Institutes of Health, Rockville, MD). The cell viability was defined as the percentage of live cell area(s) divided by the sum of both live and dead cell area of each islet. Briefly, the z-stack fluorescent images of whole islet(s) acquired from the live/dead staining were projected onto a 2D image using maximum intensity projection. The channels were then individually split and thresholded to determine the area of the live cells and dead cells. The region of interest for each islet was selected manually and was kept consistent when determining the area in a different channel. Image analysis was performed on live/dead results from more than three different rodent islet isolations (≥50 distinct samples) at both 24 and 72 hours of culture period. Spatiotemporal time course and toxicity study live cell imaging was acquired using a Leica adaptive focus control to minimize focal drifts. Analysis of the area of apoptotic and dead cells was defined as the percentage area of fluorescence signal within an entire islet area, which was selected from a corresponding bright-field image. Notably, to obtain consistency in the percentage area quantifications between each image, an auto local threshold algorithm called "Moments" was used. Additional correction for the focal drifts was performed using a HyperStackReg ImageJ plugin. Icy software for bioimage informatics (Institut Pasteur and France-BioImaging, France) was used to create superimposed color maps of time-course images using an active contours detection. For general Ca^{2+} imaging analysis, more than 12 individual cells from at least three islets were selected and their region was tracked and interpolated overtime. Subsequently, their mean fluorescence intensities (MFI) were obtained, normalized to the average basal MFI of the first 30-min low glucose step, and plotted as a function of time. Ca^{2+} traces for toxicity treatment were first divided by the average fluorescent values of bovine serum albumin (BSA)–treated islets and then normalized to the average basal MFI of the 30-min low glucose step before the treatment.

Evaluation of islet function

The dGSIS of the islets, rodent and human, was conducted by connecting MPS to a PERI-4.2 perifusion system (Biorep Technologies, Miami Lakes, FL). Control islets in static culture were transferred into a fresh Acry-Chip, at appropriate time points, for dGSIS assessments to ensure consistency in stimulation profiles. Standard perifusion buffer containing KRBB buffer [115 mM $NaCl_2$, 4.7 mM KCl, 1.2 mM KH_2PO_4, 1.2 mM $MgSO_4$, 2.5 mM $CaCl_2$, 26 mM $NaHCO_3$, 0.2% (w/v) BSA, and 25 mM HEPES (pH 7.4)] with a selected glucose concentration (low, 3 mM; high, 11 mM) and/or KCl (25 mM) was perifused at a constant flow rate of 30 μl/min. Specifically, islets were first stabilized using a low glucose solution for 60 min and then stimulated with a sequence of 20-min low glucose, 30-min high glucose, 30-min low glucose, 10-min KCl, and 80-min low glucose media. Analytes were collected every 2 min from the outflow tubing and immediately stored at −80°C. Insulin concentrations were quantified using commercially available ELISA kits (Mercodia, Sweden). The values were first converted to micrograms per liter units. They were then converted to picograms per minute using the constant flow rate as listed above, normalized to the number of handpicked islets, and plotted as a function of time. The dead volume within the circulation tubing and islet MPS channels induced a lag of ~8 min. Hence, all dGSIS plots were denoted with 3G, 11G, and/or KCl to represent the stimulation times executed by the perifusion system with an inclusion of the calculated dead volume delay. AUC of an entire region of high glucose, beyond the denoted regions illustrated in the dGSIS plots, was calculated. The peak values were normalized to the corresponding average glucose baseline levels for AUC calculations. Notably, during serial assessments of the islet functionality, the dGSIS performed at earlier time points (i.e., 24, 48, and/or 72 hours) did not include the KCl stimulation step to preserve islet health.

Additional pancreatic hormone secretions were measured using a MILLIPLEX MAP rat metabolic hormone magnetic bead panel–metabolism multiplex assay (MilliporeSigma, Burlington, MA). The assay was performed by following the manufacturers' recommended protocol with inclusion of proper standards and quality control samples.

The antibody-immobilized bead cocktail contained analytes to capture glucagon, active GLP-1, C-peptide, and active amylin. The samples were ran on Luminex MAGPIX system (Luminex Corp., Austin, TX) and the median fluorescent intensity data were analyzed using a five-parameter logistic curve-fitting method to calculate analyte concentration in samples.

Viral transduction and Ca^{2+} imaging toxicity study

Rodent islets were transduced with GCaMP6m adenovirus type 5 (catalog no. 1909, Vector Biolabs, Malvern, PA) at a multiplicity of infection of 500 on the day of procurement (*28*). Islets were assumed to contain 1500 cells per IEQ and were used for experiments 48 hours after viral transduction (*69*). GCaMP-transfected islets were embedded in hydrogels and assembled in Acry-Chip for continuous perifusion and live-cell imaging, as described above. The emission from the Ca^{2+}-bound fluorescent protein within the GCaMP islet was detected with Fluo-4 (ex/em, ~494/~506 nm). Islets were first stabilized using a working solution of low-glucose CMRL culture media for 90 min and then stimulated with a sequence of 30-min low CMRL, 30-min high CMRL, 70-min low CMRL, and 150 min of glucolipotoxic agent. 1 mM of Sodium palmitate (Acros Organics, Fair Lawn, NJ) and 0.17 mM fatty acid–free BSA (Roche, Switzerland) were conjugated at 6:1 ratio, respectively, in 116.36 mM sodium chloride solution following a protocol from Seahorse Bioscience. Fatty acid–free BSA (0.17 mM) alone was also prepared for use as a control. The preparation of CMRL culture media used for toxicity study was slightly modified to achieve consistency in buffer compositions and osmolarities. Stock low glucose 2× CMRL 1066–based media without L-glutamine and phenol red was prepared from powder (USBiological, Salem, MA) and supplemented with 20% fetal bovine serum (HyClone Laboratories, Logan, UT), 50 mM HEPES, 4 mM L-glutamine, 2% penicillin-streptomycin, and 22.2 mM D-mannitol (all from Sigma-Aldrich, St. Louis, MO). Similarly, stock high glucose 2× CMRL media was prepared and supplemented with 22.2 mM D-glucose instead of D-mannitol. Working solution of low and high glucose 1× CMRL media were prepared by performing 1:1 dilutions of respective stock 2× CMRL media and 0.17 mM fatty acid–free BSA. The final working solution of both low- and high-glucose CMRL media had 5.6 and 16.7 mM glucose concentrations, respectively. Their calculated osmolarity was found to be roughly 323.9 mOsm/liter.

Statistical methods

The statistical analyses were performed using GraphPad Prism 8.2 software (GraphPad Software, San Diego, CA). Statistical analysis used were unpaired parametric *t* test with Welch's correction, one-way ANOVA with Browne-Forsythe and Welch tests corrected for multiple comparisons using Games-Howell approach for $n > 50$ samples or either Dunnett T3 or Tamhane T2 approach for $n < 50$ samples, and two-way ANOVA with matching factors corrected for multiple comparisons using either Sidak's or Tukey's post hoc pairwise comparison test. In addition, a robust regression and outlier removal (ROUT) test was performed where *Q*, the chance of identifying one or more outliers, was set to 1% unless otherwise noted. For cellular death tracking analysis, we used Geisser-Greenhouse correction without sphericity. The pooled rodent functionality results and glucagon secretion results were analyzed by fitting a mixed model to account for missing values in the time course; results could then be interpreted similar to repeated-measures ANOVA with the assumption of sphericity. A confidence level of 95% was considered significant with designations of $^{*}P < 0.05$, $^{**}P < 0.01$, $^{***}P < 0.001$, and $^{****}P < 0.0001$ (two-tailed). Results without statistical significance denoted can be assumed to be of no significant difference. All values were expressed as means ± SD, and corresponding *P* values and their statistical analyses are reported in individual figure captions. The details of statistics are also listed in table S2. Both rodent and human islet culture experiments using distinct islet batch preparations were repeated at least three times to validate trends.

SUPPLEMENTARY MATERIALS

Supplementary material for this article is available at http://advances.sciencemag.org/cgi/content/full/7/7/eaba5515/DC1

View/request a protocol for this paper from *Bio-protocol*.

REFERENCES AND NOTES

1. M. Weatherall, An end to the search for new drugs? *Nature* **296**, 387–390 (1982).
2. S. Breslin, L. O'Driscoll, Three-dimensional cell culture: The missing link in drug discovery. *Drug Discov. Today* **18**, 240–249 (2013).
3. A. Ranga, N. Gjorevski, M. P. Lutolf, Drug discovery through stem cell-based organoid models. *Adv. Drug Deliv. Rev.* **69–70**, 19–28 (2014).
4. N. J. Hart, A. C. Powers, Use of human islets to understand islet biology and diabetes: Progress, challenges and suggestions. *Diabetologia* **62**, 212–222 (2019).
5. C. Ricordi, J. S. Goldstein, A. N. Balamurugan, G. L. Szot, T. Kin, C. Liu, C. W. Czarniecki, B. Barbaro, N. D. Bridges, J. Cano, W. R. Clarke, T. L. Eggerman, L. G. Hunsicker, D. B. Kaufman, A. Khan, D.-E. Lafontant, E. Linetsky, X. Luo, J. F. Markmann, A. Naji, O. Korsgren, J. Oberholzer, N. A. Turgeon, D. Brandhorst, X. Chen, A. S. Friberg, J. Lei, L.-J. Wang, J. J. Wilhelm, J. Willits, X. Zhang, B. J. Hering, A. M. Posselt, P. G. Stock, A. M. J. Shapiro, X. Chen, National Institutes of Health-sponsored clinical islet transplantation consortium phase 3 trial: Manufacture of a complex cellular product at eight processing facilities. *Diabetes* **65**, 3418–3428 (2016).
6. K. K. Papas, H. De Leon, T. M. Suszynski, R. C. Johnson, Oxygenation strategies for encapsulated islet and beta cell transplants. *Adv. Drug Deliv. Rev.* **139**, 139–156 (2019).
7. L. Rosenberg, R. Wang, S. Paraskevas, D. Maysinger, Structural and functional changes resulting from islet isolation lead to islet cell death. *Surgery* **126**, 393–398 (1999).
8. D. W. Scharp, P. Marchetti, Encapsulated islets for diabetes therapy: History, current progress, and critical issues requiring solution. *Adv. Drug Deliv. Rev.* **67-68**, 35–73 (2014).
9. K. Y. Lee, D. J. Mooney, Alginate: Properties and biomedical applications. *Prog. Polym. Sci.* **37**, 106–126 (2012).
10. J. W. Haycock, in *3D Cell Culture* (Springer, 2011), pp. 1–15.
11. S. N. Bhatia, D. E. Ingber, Microfluidic organs-on-chips. *Nat. Biotechnol.* **32**, 760–772 (2014).
12. S. K. Sia, G. M. Whitesides, Microfluidic devices fabricated in poly(dimethylsiloxane) for biological studies. *Electrophoresis* **24**, 3563–3576 (2003).
13. D. Hoelzle, M. Lake, C. Narciso, K. Cowdrick, T. Storey, S. Zhang, J. Zartman, Microfluidic device design, fabrication, and testing protocols. *Protoc. Exch.* 10.1038/protex.2015.069, (2015).
14. G. Lenguito, D. Chaimov, J. R. Weitz, R. Rodriguez-Diaz, S. A. K. Rawal, A. Tamayo-Garcia, A. Caicedo, C. L. Stabler, P. Buchwald, A. Agarwal, Resealable, optically accessible, PDMS-free fluidic platform for ex vivo interrogation of pancreatic islets. *Lab Chip* **17**, 772–781 (2017).
15. P. Buchwald, A local glucose-and oxygen concentration-based insulin secretion model for pancreatic islets. *Theor. Biol. Med. Model.* **8**, 20 (2011).
16. C. Ricordi, D. W. R. Gray, B. J. Hering, D. B. Kaufman, G. L. Warnock, N. M. Kneteman, S. P. Lake, N. J. M. London, C. Socci, R. Alejandro, Y. Zeng, D. W. Scharp, G. Viviani, L. Falqui, A. Tzakis, R. G. Bretzel, K. Federlin, G. Pozza, R. F. L. James, R. V. Rajotte, V. Di Carlo, P. J. Morris, D. E. R. Sutherland, T. E. Starzl, D. H. Mintz, P. E. Lacy, Islet isolation assessment in man and large animals. *Acta Diabetol. Lat.* **27**, 185–195 (1990).
17. M. M. Coronel, R. Geusz, C. L. Stabler, Mitigating hypoxic stress on pancreatic islets via in situ oxygen generating biomaterial. *Biomaterials* **129**, 139–151 (2017).
18. P.-O. Carlsson, P. Liss, A. Andersson, L. Jansson, Measurements of oxygen tension in native and transplanted rat pancreatic islets. *Diabetes* **47**, 1027–1032 (1998).
19. R. Olsson, P.-O. Carlsson, A low-oxygenated subpopulation of pancreatic islets constitutes a functional reserve of endocrine cells. *Diabetes* **60**, 2068–2075 (2011).
20. E. S. Avgoustiniatos, "Oxygen diffusion limitations in pancreatic islet culture and immunoisolation," thesis, Massachusetts Institute of Technology, Cambridge, MA (2002).
21. K. E. Dionne, C. K. Colton, M. L. Lyarmush, Effect of hypoxia on insulin secretion by isolated rat and canine islets of Langerhans. *Diabetes* **42**, 12–21 (1993).

22. P. Rorsman, L. Eliasson, E. Renström, J. Gromada, S. Barg, S. Göpel, The cell physiology of biphasic insulin secretion. *Physiology* **15**, 72–77 (2000).
23. A. F. Adewola, D. Lee, T. Harvat, J. Mohammed, D. T. Eddington, J. Oberholzer, Y. Wang, Microfluidic perifusion and imaging device for multi-parametric islet function assessment. *Biomed. Microdevices* **12**, 409–417 (2010).
24. O. Cabrera, M. C. Jacques-Silva, D. M. Berman, A. Fachado, F. Echeverri, R. Poo, A. Khan, N. S. Kenyon, C. Ricordi, P.-O. Berggren, A. Caicedo, Automated, high-throughput assays for evaluation of human pancreatic islet function. *Cell Transplant.* **16**, 1039–1048 (2008).
25. K. Maedler, J. Oberholzer, P. Bucher, G. A. Spinas, M. Y. Donath, Monounsaturated fatty acids prevent the deleterious effects of palmitate and high glucose on human pancreatic β-cell turnover and function. *Diabetes* **52**, 726–733 (2003).
26. V. Poitout, R. P. Robertson, Minireview: Secondary β-cell failure in type 2 diabetes—A convergence of glucotoxicity and lipotoxicity. *Endocrinology* **143**, 339–342 (2002).
27. R. P. Robertson, J. Harmon, P. O. T. Tran, V. Poitout, β-Cell glucose toxicity, lipotoxicity, and chronic oxidative stress in type 2 diabetes. *Diabetes* **53**, S119–S124 (2004).
28. T.-W. Chen, T. J. Wardill, Y. Sun, S. R. Pulver, S. L. Renninger, A. Baohan, E. R. Schreiter, R. A. Kerr, M. B. Orger, V. Jayaraman, L. L. Looger, K. Svoboda, D. S. Kim, Ultrasensitive fluorescent proteins for imaging neuronal activity. *Nature* **499**, 295–300 (2013).
29. B. J. van Meer, H. de Vries, K. S. A. Firth, J. van Weerd, L. G. J. Tertoolen, H. B. J. Karperien, P. Jonkheijm, C. Denning, A. P. IJzerman, C. L. Mummery, Small molecule absorption by PDMS in the context of drug response bioassays. *Biochem. Biophys. Res. Commun.* **482**, 323–328 (2017).
30. M. Adiraj Iyer, D. T. Eddington, Storing and releasing rhodamine as a model hydrophobic compound in polydimethylsiloxane microfluidic devices. *Lab Chip* **19**, 574–579 (2019).
31. A. L. Glieberman, B. D. Pope, J. F. Zimmerman, Q. Liu, J. P. Ferrier Jr., J. H. R. Kenty, A. M. Schrell, N. Mukhitov, K. L. Shores, A. B. Tepole, D. A. Melton, M. G. Roper, K. K. Parker, Synchronized stimulation and continuous insulin sensing in a microfluidic human Islet on a Chip designed for scalable manufacturing. *Lab Chip* **19**, 2993–3010 (2019).
32. E. Berthier, E. W. K. Young, D. Beebe, Engineers are from PDMS-land, biologists are from polystyrenia. *Lab Chip* **12**, 1224–1237 (2012).
33. K. Ren, W. Dai, J. Zhou, J. Su, H. Wu, Whole-Teflon microfluidic chips. *Proc. Natl. Acad. Sci. U.S.A.* **108**, 8162–8166 (2011).
34. I. R. Sweet, D. L. Cook, R. W. Wiseman, C. J. Greenbaum, Å. Lernmark, S. Matsumoto, J. C. Teague, K. A. Krohn, Dynamic perifusion to maintain and assess isolated pancreatic islets. *Diabetes Technol. Ther.* **4**, 67–76 (2002).
35. P. Buchwald, A. Tamayo-Garcia, V. Manzoli, A. A. Tomei, C. L. Stabler, Glucose-stimulated insulin release: Parallel perifusion studies of free and hydrogel encapsulated human pancreatic islets. *Biotechnol. Bioeng.* **115**, 232–245 (2018).
36. P. Buchwald, FEM-based oxygen consumption and cell viability models for avascular pancreatic islets. *Theor. Biol. Med. Model.* **6**, 5 (2009).
37. P. Buchwald, X. Wang, A. Khan, A. Bernal, C. Fraker, L. Inverardi, C. Ricordi, Quantitative assessment of islet cell products: Estimating the accuracy of the existing protocol and accounting for islet size distribution. *Cell Transplant.* **18**, 1223–1235 (2009).
38. R. R. MacGregor, S. J. Williams, P. Y. Tong, K. Kover, W. V. Moore, L. Stehno-Bittel, Small rat islets are superior to large islets in in vitro function and in transplantation outcomes. *Am. J. Physiol. Endocrinol. Metab.* **290**, E771–E779 (2006).
39. A. P. Gilmore, Anoikis. *Cell Death Differ.* **12**, 1473–1477 (2005).
40. J. Grossmann, Molecular mechanisms of "detachment-induced apoptosis—Anoikis". *Apoptosis* **7**, 247–260 (2002).
41. S. M. Frisch, H. Francis, Disruption of epithelial cell-matrix interactions induces apoptosis. *J. Cell Biol.* **124**, 619–626 (1994).
42. J. C. Stendahl, D. B. Kaufman, S. I. Stupp, Extracellular matrix in pancreatic islets: Relevance to scaffold design and transplantation. *Cell Transplant.* **18**, 1–12 (2009).
43. K. Jiang, D. Chaimov, S. N. Patel, J.-P. Liang, S. C. Wiggins, M. M. Samojlik, A. Rubiano, C. S. Simmons, C. L. Stabler, 3-D physiomimetic extracellular matrix hydrogels provide a supportive microenvironment for rodent and human islet culture. *Biomaterials* **198**, 37–48 (2019).
44. L. A. Llacua, B. J. de Haan, P. de Vos, Laminin and collagen IV inclusion in immunoisolating microcapsules reduces cytokine-mediated cell death in human pancreatic islets. *J. Tissue Eng. Regen. Med.* **12**, 460–467 (2018).
45. K. A. Homan, N. Gupta, K. T. Kroll, D. B. Kolesky, M. Skylar-Scott, T. Miyoshi, D. Mau, M. T. Valerius, T. Ferrante, J. V. Bonventre, J. A. Lewis, R. Morizane, Flow-enhanced vascularization and maturation of kidney organoids in vitro. *Nat. Methods* **16**, 255–262 (2019).
46. Y. Jun, J. Lee, S. Choi, J. H. Yang, M. Sander, S. Chung, S.-H. Lee, In vivo–mimicking microfluidic perfusion culture of pancreatic islet spheroids. *Sci. Adv.* **5**, eaax4520 (2019).
47. J. D. Rivas-Carrillo, A. Soto-Gutierrez, N. Navarro-Alvarez, H. Noguchi, T. Okitsu, Y. Chen, T. Yuasa, K. Tanaka, M. Narushima, A. Miki, H. Misawa, Y. Tabata, H.-S. Jun, S. Matsumoto, I. J. Fox, N. Tanaka, N. Kobayashi, Cell-permeable pentapeptide V5 inhibits apoptosis and enhances insulin secretion, allowing experimental single-donor islet transplantation in mice. *Diabetes* **56**, 1259–1267 (2007).
48. O. Alcazar, P. Buchwald, Concentration-dependency and time profile of insulin secretion: Dynamic perifusion studies with human and murine islets. *Front. Endocrinol.* **10**, 680 (2019).
49. J. S. Mohammed, Y. Wang, T. A. Harvat, J. Oberholzer, D. T. Eddington, Microfluidic device for multimodal characterization of pancreatic islets. *Lab Chip* **9**, 97–106 (2009).
50. M. Skelin Klemen, J. Dolenšek, M. Slak Rupnik, A. Stožer, The triggering pathway to insulin secretion: Functional similarities and differences between the human and the mouse β cells and their translational relevance. *Islets* **9**, 109–139 (2017).
51. J. Pi, Q. Zhang, J. Fu, C. G. Woods, Y. Hou, B. E. Corkey, S. Collins, M. E. Andersen, ROS signaling, oxidative stress and Nrf2 in pancreatic beta-cell function. *Toxicol. Appl. Pharmacol.* **244**, 77–83 (2010).
52. Y.-J. Chen, T. Yamazoe, K. F. Leavens, F. L. Cardenas-Diaz, A. Georgescu, D. Huh, P. Gadue, B. Z. Stanger, iPreP is a three-dimensional nanofibrillar cellulose hydrogel platform for long-term ex vivo preservation of human islets. *JCI Insight* **4**, e124644 (2019).
53. S. Cechin, S. Álvarez-Cubela, J. A. Giraldo, R. D. Molano, S. Villate, C. Ricordi, A. Pileggi, L. Inverardi, C. A. Fraker, J. Domínguez-Bendala, Influence of in vitro and in vivo oxygen modulation on β cell differentiation from human embryonic stem cells. *Stem Cells Transl. Med.* **3**, 277–289 (2014).
54. C. A. Fraker, S. Álvarez, P. Papadopoulos, J. Giraldo, W. Gu, C. Ricordi, L. Inverardi, J. Domínguez-Bendala, Enhanced oxygenation promotes β-cell differentiation in vitro. *Stem Cells* **25**, 3155–3164 (2007).
55. M. M. F. Qadir, S. Álvarez-Cubela, J. Weitz, J. K. Panzer, D. Klein, Y. Moreno-Hernández, S. Cechin, A. Tamayo, J. Almaça, H. Hiller, M. Beery, I. Kusmartseva, M. Atkinson, S. Speier, C. Ricordi, A. Pugliese, A. Caicedo, C. A. Fraker, R. L. Pastori, J. Domínguez-Bendala, Long-term culture of human pancreatic slices as a model to study real-time islet regeneration. *Nat. Commun.* **11**, 3265 (2020).
56. C. Gravena, P. C. Mathias, S. J. H. Ashcroft, Acute effects of fatty acids on insulin secretion from rat and human islets of Langerhans. *J. Endocrinol.* **173**, 73–80 (2002).
57. C. S. Olofsson, S. Collins, M. Bengtsson, L. Eliasson, A. Salehi, K. Shimomura, A. Tarasov, C. Holm, F. Ashcroft, P. Rorsman, Long-term exposure to glucose and lipids inhibits glucose-induced insulin secretion downstream of granule fusion with plasma membrane. *Diabetes* **56**, 1888–1897 (2007).
58. I. T. Kuok, A. M. Rountree, S.-R. Jung, I. R. Sweet, Palmitate is not an effective fuel for pancreatic islets and amplifies insulin secretion independent of calcium release from endoplasmic reticulum. *Islets* **11**, 51–64 (2019).
59. S. Xu, S. M. Nam, J.-H. Kim, R. Das, S.-K. Choi, T. T. Nguyen, X. Quan, S. J. Choi, C. H. Chung, E. Y. Lee, I.-K. Lee, A. Wiederkehr, C. B. Wollheim, S.-K. Cha, K.-S. Park, Palmitate induces ER calcium depletion and apoptosis in mouse podocytes subsequent to mitochondrial oxidative stress. *Cell Death Dis.* **6**, e1976 (2015).
60. M. Nemecz, A. Constantin, M. Dumitrescu, N. Alexandru, A. Filippi, G. Tanko, A. Georgescu, The distinct effects of palmitic and oleic acid on pancreatic beta cell function: The elucidation of associated mechanisms and effector molecules. *Front. Pharmacol.* **9**, 1554 (2019).
61. C. Warnotte, P. Gilon, M. Nenquin, J.-C. Henquin, Mechanisms of the stimulation of insulin release by saturated fatty acids: A study of palmitate effects in mouse β-cells. *Diabetes* **43**, 703–711 (1994).
62. M. Garcia-Contreras, A. Tamayo-Garcia, K. L. Pappan, G. A. Michelotti, C. L. Stabler, C. Ricordi, P. Buchwald, Metabolomics study of the effects of inflammation, hypoxia, and high glucose on isolated human pancreatic islets. *J. Proteome Res.* **16**, 2294–2306 (2017).
63. E. A. Phelps, C. Cianciaruso, I. P. Michael, M. Pasquier, J. Kanaani, R. Nano, V. Lavallard, N. Billestrup, J. A. Hubbell, S. Baekkeskov, Aberrant accumulation of the diabetes autoantigen GAD65 in Golgi membranes in conditions of ER stress and autoimmunity. *Diabetes* **65**, 2686–2699 (2016).
64. H. L. Lanz, A. Saleh, B. Kramer, J. Cairns, C. P. Ng, J. Yu, S. J. Trietsch, T. Hankemeier, J. Joore, P. Vulto, R. Weinshilboum, L. Wang, Therapy response testing of breast cancer in a 3D high-throughput perfused microfluidic platform. *BMC Cancer* **17**, 709 (2017).
65. E. L. Moreno, S. Hachi, K. Hemmer, S. J. Trietsch, A. S. Baumuratov, T. Hankemeier, P. Vulto, J. C. Schwamborn, R. M. T. Fleming, Differentiation of neuroepithelial stem cells into functional dopaminergic neurons in 3D microfluidic cell culture. *Lab Chip* **15**, 2419–2428 (2015).
66. M. Jang, P. Neuzil, T. Volk, A. Manz, A. Kleber, On-chip three-dimensional cell culture in phaseguides improves hepatocyte functions in vitro. *Biomicrofluidics* **9**, 034113 (2015).
67. S. Bauer, C. Wennberg Huldt, K. P. Kanebratt, I. Durieux, D. Gunne, S. Andersson, L. Ewart, W. G. Haynes, I. Maschmeyer, A. Winter, C. Ämmälä, U. Marx, T. B. Andersson, Functional coupling of human pancreatic islets and liver spheroids on-a-chip: Towards a novel human ex vivo type 2 diabetes model. *Sci. Rep.* **7**, 14620 (2017).
68. R. Bottino, L. A. Fernandez, C. Ricordi, R. Lehmann, M. F. Tsan, R. Oliver, L. Inverardi, Transplantation of allogeneic islets of Langerhans in the rat liver: Effects of macrophage depletion on graft survival and microenvironment activation. *Diabetes* **47**, 316–323 (1998).
69. A. Pisania, G. C. Weir, J. J. O'Neil, A. Omer, V. Tchipashvili, J. Lei, C. K. Colton, S. Bonner-Weir, Quantitative analysis of cell composition and purity of human pancreatic islet preparations. *Lab. Invest.* **90**, 1661–1675 (2010).

Acknowledgments: We would like to thank I. Labrada-Miravet for excellent technical assistance during rodent islet procurement and experiments. For additional assistance during experiments, we would like to thank M. M. Samojlik, E. Vishka, and A. E. Widener from UF Department of Biomedical Engineering and O. Alcazar from the UM Diabetes Research Institute. We would also like to acknowledge the families of those who donated organs for their invaluable contribution to science. **Funding:** This study was funded by the NIDDK-supported Human Islet Research Network (HIRN; https://hirnetwork.org/; UC4 DK104208 and UG3 DK122638). M.I. was funded by F31DK118860. Human pancreatic islets were provided by the NIDDK-funded IIDP at City of Hope (2UC4DK098085) and the Human Islet Cell Processing Facility at the Diabetes Research Institute (University of Miami Miller School of Medicine, Miami, FL). **Author contributions:** S.N.P., M.I., D.C., A.A., and C.L.S. conceived and designed the study. M.I. and A.A. designed and fabricated the MPS platform. S.N.P., M.I., and D.C. designed the MPS workflow with supervision from A.A. and C.L.S. M.I. and P.B. developed the in silico models. S.N.P., D.C., and C.L.S. performed biological validations. S.N.P. developed imaging strategies and performed imaging experiments and analysis for viability imaging, spatiotemporal tracking, and toxicity study. E.A.P. contributed in both time-course image acquisitions and analysis and Ca^{2+} imaging toxicity study. D.W.H. performed viral transduction of rodent islets and contributed in analysis of Ca^{2+} imaging toxicity study. S.N.P. and D.C. performed islet functionality assessments with contributions from A.V. and D.L. S.N.P. performed the multiplex metabolic hormonal assays. S.N.P. and M.I. performed overall data acquisition, analysis, and visualization. S.N.P., M.I., A.A., and C.L.S. wrote the manuscript with input from other authors. All authors read and approved the final version of the manuscript. C.L.S. and A.A. acquired the funding. **Competing interests:** A.A. is an inventor on a pending patent related to this work filed by the University of Miami (no. 15/766614, filed 6 October 2016) and licensed by Bio-Vitro Inc. M.I. and A.A. are cofounders of Bio-Vitro Inc., which is currently negotiating a licensing agreement with the University of Miami for the microfluidic chip intellectual property. The authors declare that they have no other competing interests. **Data and materials availability:** All data needed to evaluate the conclusions in the paper are present in the paper and/or the Supplementary Materials. Additional data related to this paper may be requested from the corresponding authors. Chips and associated microfluidic supplies can be provided by A.A. pending scientific review and a completed material transfer agreement. Requests for the chips and associated microfluidic supplies should be submitted to a.agarwal2@miami.edu.

Submitted 12 December 2019
Accepted 23 December 2020
Published 12 February 2021
10.1126/sciadv.aba5515

Citation: S. N. Patel, M. Ishahak, D. Chaimov, A. Velraj, D. LaShoto, D. W. Hagan, P. Buchwald, E. A. Phelps, A. Agarwal, C. L. Stabler, Organoid microphysiological system preserves pancreatic islet function within 3D matrix. *Sci. Adv.* **7**, eaba5515 (2021).

ScienceAdvances

Organoid microphysiological system preserves pancreatic islet function within 3D matrix

S. N. Patel, M. Ishahak, D. Chaimov, A. Velraj, D. LaShoto, D. W. Hagan, P. Buchwald, E. A. Phelps, A. Agarwal, and C. L. Stabler

Sci. Adv., **7** (7), eaba5515.
DOI: 10.1126/sciadv.aba5515

Science Advances (ISSN 2375-2548) is published by the American Association for the Advancement of Science. 1200 New York Avenue NW, Washington, DC 20005. The title *Science Advances* is a registered trademark of AAAS.